Politecnico di Torino

Master’s Degree in Automotive Engineering
Product Design – A.Y. 2025/2026
July 2026

Reverse Engineering and Functional Analysis of a Crescent Internal Gear Pump

Supervisor:
Massimo Rundo

Candidate:
Simone Pizzola

Index

Abstract 3
1. Introduction 4
1.1 Application Context of Hydraulic Pumps 4
1.2 Objectives of the Thesis 4
1.3 Methodology 5
2. State of the Art on Crescent Pumps 5
2.1 Operating Principle 5
2.2 Analytical Modelling of Flow Rate 7
2.3 Volumetric Efficiency and Leakage Phenomena 8
2.4 Lumped Parameter Modelling and Dynamic Simulation 9
2.5 Mechanical Effects and Gear Micro-Motion 11
2.6 Gear Profile Design and Geometric Optimization 12
2.7 Flow Ripple and Noise Generation 13
2.8 Trapped Oil Phenomena and Pressure Peaks 14
2.9 Relations to the Present Thesis 15
3. Pump Description and Technical Specifications 16
3.1 Pump Main Specifications 16
3.2 Pump Functional Overview 17
4. Reverse Engineering and Parameters Identification 20
4.1 Data Acquisition and Measurement Tools 20
4.2 CAD Modelling of the Pump Assembly 21
4.2.1 Pump Housing 21
4.2.2 Compensation Plates and Plates Gaskets 22
4.2.3 Crescent Elements 24
4.2.4 Internal Gearset 25
5. Performance Evaluation 30
5.1 Input Parameters 30
5.2 Active Meshing Segment 31
5.3 Auxiliary Angular Variables 33
5.4 Radius Vectors for the Control Volumes 37
5.5 Control Volume Derivatives 39
5.6 Flow Rate and Flow Ripple Calculation 44
5.7 Pump Displacement 46

6 Functional Analysis *47*
6.1 Beginning of the Meshing Cycle 47
6.2 Expansion Phase and Suction Process 49
6.3 Transport of the Fluid Along the Crescent 50
6.4 Compression Phase and Delivery Process 51
7 Results *56*
7.1 Discussion and Comparison with Manufacturer Data 56
8 Conclusions *58*
Appendix A: MATLAB Code *59*
Bibliography *65*

Abstract

Crescent pumps are a particular type of internal gear pumps and are extensively employed in fluid power applications because of their compact architecture and capability to work efficiently at elevated pressures and rotational speeds. Owing to these features, they are particularly well suited for automotive systems, especially for engine lubrication applications.
However, accurately predicting the performance of these pumps is still a complex task, since their behaviour is strongly influenced by the interaction between geometric characteristics, fluid properties, and operating conditions. In particular, key performance indicators such as flow rate, volumetric efficiency, and flow ripple are strongly influenced by internal leakage and the detailed geometry of the pump components. This thesis presents a methodology for the analysis of a specific internal gear pump based on the integration of reverse engineering, 3D modelling techniques and mathematical models. Firstly, the geometry of the pump is reconstructed through measurements and CAD modelling, allowing the identification of the main design parameters and then an analytical model is implemented to evaluate the variation of chamber volumes during rotation and to predict the main parameters of the pump. The proposed approach is implemented in MATLAB and the results demonstrate that the combination of reverse engineering and analytical modelling provides a simple and effective tool for performance prediction, offering a good balance between accuracy and computational efficiency.

1. Introduction

1.1 Application Context of Hydraulic Pumps

Hydraulic pumps are widely employed in modern engineering systems because they provide high power density, compactness, reliability, and precise controllability. Among the different pump technologies, internal gear pumps are particularly appreciated for their smooth operation, low noise emission, and capability to operate under high-pressure conditions. These characteristics make them suitable for a broad range of industrial and automotive applications. In automotive engineering, hydraulic pumps are extensively used in lubrication circuits, transmission systems, steering assistance, and cooling architectures. In particular, crescent-type internal gear pumps are commonly adopted as engine oil pumps due to their compact dimensions and their ability to ensure a stable flow rate over a wide range of rotational speeds. The growing demand for energy efficiency and emission reduction has further increased the importance of optimizing hydraulic pump performance, especially in applications where parasitic losses directly affect fuel consumption. The operating conditions of automotive pumps are often highly demanding. The machines must operate with large temperature variations, transient rotational speeds, and significant pressure fluctuations. Under these conditions, the volumetric efficiency of the pump becomes strongly dependent on leakage phenomena, fluid compressibility, and pressure ripple generation. For this reason, modern hydraulic pump design requires not only geometric optimization but also accurate predictive models capable of describing the internal fluid-dynamic behaviour of the machine. The increasing electrification of vehicles is also influencing the evolution of hydraulic pumps. Electrically driven lubrication and cooling pumps are progressively replacing mechanically driven systems, enabling flow regulation according to real operating demand. This trend requires highly efficient pumps capable of maintaining stable performance even at variable rotational speeds and partial load conditions. Within this framework, the accurate modelling of internal gear pumps becomes essential. The prediction of theoretical flow rate, flow ripple, trapped volume evolution, and leakage mechanisms represents a crucial step for the optimization of pump efficiency and acoustic behaviour. Consequently, the development of analytical and numerical models, combined with reverse engineering methodologies, plays a central role in modern hydraulic pump research and design.

1.2 Objectives of the Thesis

The main objective of this thesis is to develop a systematic methodology for the reconstruction and analysis of an internal gear pump starting from a physical component and limited available data. More specifically, the work aims to:

- Reconstruct a consistent three-dimensional model of the pump through a reverse engineering approach based on direct measurements and CAD modelling
- Identify the main geometric and kinematic parameters of the gear set, including module, number of teeth, pressure angle, and characteristic radii
- Analyse the internal fluid domains and describe the evolution of the volumes enclosed between gear teeth during operation
- Estimate the theoretical displacement and flow rate of the pump through a discrete volumetric approach

- Compare the obtained results with the data provided by the manufacturer in order to validate the proposed methodology.

1.3 Methodology

The methodology adopted in this work is based on the integration of experimental observations, geometric reconstruction, and analytical modelling. The first phase consists in the acquisition of geometric data from the actual component. Direct measurements are performed using a vernier caliper, while additional information is obtained from the manufacturer datasheet. Due to the complexity of certain components, a complementary two-dimensional scanning approach is employed to capture relevant geometric features. In the second phase, the acquired data are used to develop a parametric three-dimensional model of the pump with a the CAD software Solidworks. The model includes the main components of the machine, such as the inner and outer gears, the crescent element, and the lateral surfaces associated with the compensation plates. Once the geometry is reconstructed, a parameter identification procedure is carried out in order to estimate the main characteristics of the gear set. This step combines direct measurements with standard gear theory relations and, when necessary, with the comparison between the reconstructed tooth profile and the theoretical involute curve. The identified parameters are then used to define the internal fluid domains and to analyse the evolution of the control volumes as a function of the angular position of the pinion gear. A discrete approach is adopted to evaluate the variation of the enclosed volumes, allowing the estimation of the theoretical displacement and flow rate of the pump. Finally, as said before, the results obtained from the model are compared with the manufacturer data, providing a validation and a discussion of the adopted approach.

2. State of the Art on Crescent Pumps

2.1 Operating Principle

Crescent-type internal gear pumps belong to the class of positive displacement machines and are widely employed in fluid power systems, particularly in automotive lubrication and hydraulic actuation applications. Their operating principle is based on the controlled transport of fluid through the periodic variation of discrete chamber volumes formed between meshing gears. From a constructive point of view, the pump consists of a inner pinion, which acts as the driving element, and a ring, which is driven through an internal gear meshing. The number of teeth of the outer rotor exceeds that of the inner rotor by one unit, thus generating a sequence of inter-tooth chambers whose volume evolves continuously during rotation. A crescent-shaped separator is positioned between the two rotors and plays a crucial role in ensuring hydraulic separation between the suction and delivery regions.

As shown in ***Figure 2.1***, during operation, the rotation of the gears generates two distinct regions within the pump corresponding to two different ports:

- a **suction zone**, where the volume of the inter-tooth chambers increases, causing a pressure drop that draws fluid into the pump
- a **delivery zone**, where the chamber volume decreases, resulting in fluid compression and discharge toward the outlet

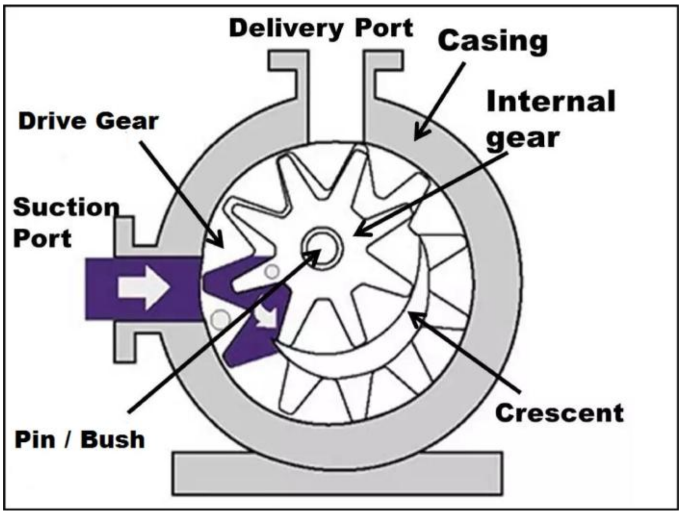

Figure 2.1 - Crescent pump basic scheme

From a mathematical point of view, the instantaneous flow rate can be expressed as the time derivative of the total volume enclosed within all active chambers:

$$Q(t) = \frac{dV_{tot}(t)}{dt} \tag{2.1}$$

This formulation, which will be described in greater detail in *Chapter 2.8* and extensively discussed in [2], establishes a direct link between geometry and flow generation, highlighting the fundamental role of the kinematic evolution of the gear pair. However, the ideal operating principle assumes perfect sealing between chambers, which is not achievable in real machines. In practice, leakage flows occur through clearances between gears, casing, and the crescent plate, leading to a reduction in the effective delivered flow rate. These phenomena are typically addressed through lumped parameter models, as discussed in [1]. Another important aspect of the operating principle is the presence of trapped volumes. During the meshing process, small fluid volumes can become temporarily isolated between adjacent teeth. As these volumes are subsequently reduced, significant pressure peaks may arise. This effect has been investigated in [5], where it is shown that the compression of trapped fluid can lead to noise generation and increased mechanical stress. Moreover, due to the discrete nature of the chamber formation, the flow rate is inherently non-uniform. The resulting oscillations, commonly referred to as flow ripple, are superimposed on the mean flow rate and represent a key aspect in the design of low-noise pumps. The analysis of such phenomena is addressed in [7], where the influence of geometric parameters and phase relationships is highlighted. In summary, the operating principle of crescent pumps is governed by a complex interaction between geometry, kinematics, and fluid dynamics. While the fundamental mechanism is relatively simple, an accurate description of the pump behaviour requires accounting for leakage, compressibility effects, and dynamic pressure variations.

2.2 Analytical Modelling of Flow Rate

The analytical modelling of flow rate in crescent pumps represents one of the most investigated topics in the literature, as it provides a direct and computationally efficient way to predict pump performance based solely on geometric parameters. A fundamental contribution in this field is provided in [2], where a rigorous formulation of the instantaneous flow rate is developed based on the variation of the inter-tooth chamber volumes during gear rotation. For a generic chamber, the instantaneous flow rate can be expressed as:

$$Q = \frac{dV}{dt} \tag{2.2}$$

Since the chamber volume is a function of the angular position of the driving gear, the chain rule gives:

$$Q(\theta) = \frac{dV}{d\theta}\frac{d\theta}{dt} \tag{2.3}$$

which leads to:

$$Q(\theta) = \omega \frac{dV(\theta)}{d\theta} \tag{2.4}$$

where θ is the angular position of the driving gear and ω is the shaft angular velocity.

However, not all chambers contribute to the delivery flow rate at a given instant. Chambers located in the suction region are characterized by an increasing volume and therefore do not deliver fluid to the outlet port. Conversely, chambers located in the delivery region undergo a volume reduction and actively contribute to the flow discharged by the pump. Following this distinction, an auxiliary variable F_i is introduced for the i-th chamber:

$$F_i = \begin{cases} -\dfrac{dV_i}{d\theta} & \text{if } \dfrac{dV_i}{d\theta} < 0 \\ 0 & \text{if } \dfrac{dV_i}{d\theta} > 0 \end{cases} \tag{2.5}$$

where V_i is the instantaneous volume of the i-th chamber.

The flow rate delivered by the i-th chamber is therefore:

$$Q_i = \omega F_i \tag{2.6}$$

and the total theoretical flow rate is obtained by summing the contributions of all chambers connected to the delivery region:

$$Q(\theta) = \omega \sum_{i=1}^{N} F_i\,(\theta) \tag{2.7}$$

It should be noted that the summation is not performed over all chamber volume derivatives. If both suction and delivery chambers were considered simultaneously, the positive and negative contributions would compensate each other, since the total fluid volume enclosed within the pump remains approximately constant. Therefore, only chambers characterized by a negative volume derivative are considered since only these chambers contribute to the outlet flow rate. This formulation allows capturing the periodic nature of the flow rate, which is characterized by oscillations around a mean value. The amplitude and frequency of these oscillations depend on the number of teeth and on the geometric configuration of the pump. A broader overview of analytical and numerical approaches is provided in [8], where different modelling techniques for gear pumps are compared. It is highlighted that analytical models offer a clear physical interpretation and low computational cost, making them particularly suitable for preliminary design and reverse engineering applications. Despite their advantages, analytical models are inherently limited by the simplifying assumptions on which they are based. In particular, they typically neglect leakage flows, fluid compressibility, and mechanical deformations. As a result, the predicted flow rate corresponds to the theoretical value, which may differ significantly from experimental measurements. For this reason, analytical models are often used as a baseline for further refinements, such as lumped parameter models or CFD simulations.

2.3 Volumetric Efficiency and Leakage Phenomena

Volumetric efficiency represents one of the most important performance indicators for positive displacement pumps, as it quantifies the deviation between the theoretical flow rate and the actual delivered flow rate. It is defined as:

$$\eta_v = \frac{Q_{real}}{Q_{theoretical}} \tag{2.8}$$

where:

- $Q_{theoretical}$ is obtained from analytical models
- Q_{real} accounts for all loss mechanisms

The main cause of volumetric losses in crescent pumps is **internal leakage**, which occurs through clearances between moving and stationary components. These leakage paths can be classified into:

- **radial leakage**, between gear tips and casing
- **axial leakage**, between gear faces and side plates
- **inter-tooth leakage**, between adjacent chambers

A simplified expression for leakage flow can be derived from laminar flow theory in thin gaps:

$$Q_{leak} = \frac{bh^3}{12\mu L}\Delta p \tag{2.9}$$

where:

- h is the clearance height
- μ is the dynamic viscosity
- Δp is the pressure difference

This relationship highlights the strong sensitivity of leakage to the clearance dimension, as it scales with h^3. Consequently, even small variations in geometry can lead to significant changes in performance. The importance of leakage modelling is emphasized in lumped parameter approaches such as [1], where leakage flows are explicitly included in the governing equations. Moreover, as discussed in [3], mechanical effects such as gear micromotion introduce time-varying clearances, further complicating the prediction of leakage. In addition to leakage, other factors contributing to volumetric losses include:

- fluid compressibility
- trapped oil expansion and compression cycles
- temperature-dependent viscosity variations

The combined effect of these phenomena results in a reduction of the effective delivered flow rate and in a deviation from the ideal performance predicted by analytical models. From a design perspective, several strategies are employed to improve volumetric efficiency:

- minimization of clearances
- optimization of gear and crescent geometry [4], [6]
- implementation of compensation mechanisms

2.4 Lumped Parameter Modelling and Dynamic Simulation

The increasing demand for higher efficiency, reduced noise emissions and improved reliability in hydraulic machines has led to the development of more advanced modelling approaches for internal gear pumps. While purely geometric models are effective for estimating the theoretical displacement and flow ripple generated by the meshing process, they are generally unable to reproduce the real operating conditions of the machine. In particular, they neglect several important physical phenomena such as fluid compressibility, internal leakages, pressure dynamics, and structural deformations.
For this reason, many researchers introduced lumped parameter models, which describe the pump as a network of interconnected hydraulic control volumes. In this approach, each chamber is associated with a pressure variable, while the connections between adjacent chambers are modelled through equivalent hydraulic resistances and leakage paths. Among the most relevant

works in the literature, in [1] a detailed lumped parameter model for a crescent internal gear pump implemented in LMS Amesim is proposed.
The pump is divided into a set of variable control volumes corresponding to the suction region, delivery region, trapped volumes, and carry-over chambers between the teeth. The pressure evolution inside each volume is obtained by applying the mass conservation principle under compressible flow conditions:

$$\frac{dp}{dt} = \frac{\beta}{V}\left(\Sigma Q_{in} - \Sigma Q_{out} - \omega \frac{dV}{d\phi}\right) \tag{2.10}$$

where β is the fluid bulk modulus, V is the instantaneous chamber volume, and $\frac{dV}{d\phi}$ represents the variation of volume during gear rotation. This formulation highlights the strong coupling between the geometric evolution of the chambers and the hydraulic response of the machine. When the chamber volume decreases during meshing, pressure rises and fluid is delivered toward the outlet. Conversely, increasing chamber volumes generate suction conditions and draw fluid into the pump. The evaluation of the volume derivatives is therefore a key aspect of the model. In crescent pumps, these derivatives depend on the geometry of the involute tooth profiles and on the instantaneous contact points between the gears. The cited study computes these quantities through the so-called vector rays approach, which relates the chamber evolution to the radii connecting the gear centers to the contact points.
Another fundamental contribution of lumped parameter models is the inclusion of leakage phenomena. In real pumps, clearances are always present between moving and stationary components, generating internal recirculation flows that reduce volumetric efficiency. These leakages occur mainly:

- through axial clearances between gears and side plates;
- between tooth tips and crescent;
- between adjacent carry-over chambers;
- across trapped volumes during meshing.

Leakage flows are typically modelled using simplified laminar flow relations as described in Chapter 2.3. In [1] is demonstrated that the leakage between the tooth tips and the crescent is one of the dominant loss mechanisms in crescent pumps. The study also showed the importance of considering the elastic deformation of the cover plate, since pressure-induced deflections modify the axial clearances and consequently alter the leakage flow rates. FEM analyses were therefore coupled with the hydraulic model to improve prediction accuracy.
In addition to steady-state flow prediction, lumped parameter approaches are widely used for the analysis of pressure ripple and dynamic behaviour. Due to fluid compressibility and trapped volume dynamics, the instantaneous outlet pressure is not constant but oscillates periodically with the gear meshing frequency. The effective bulk modulus of the oil-air mixture strongly influences the amplitude of these oscillations, making the presence of entrained air a critical factor in dynamic simulations. Compared with full CFD simulations, lumped parameter models provide lower computational costs and significantly faster simulation times, while still maintaining a good level of accuracy for engineering analyses. For this reason, they are commonly adopted during the preliminary design and optimization phases of hydraulic pumps. However, these models also present some limitations. Since the chambers are treated as lumped

volumes with uniform pressure, local three-dimensional flow phenomena cannot be fully reproduced. Similarly, cavitation effects, incomplete filling at high rotational speed, and localized pressure peaks in the meshing zone are difficult to capture accurately.

2.5 Mechanical Effects and Gear Micro-Motion

In the modelling of crescent-type internal gear pumps, the assumption of rigid and perfectly constrained components is commonly adopted in analytical formulations. However, real machines exhibit mechanical deformations and micro-motions due to the action of pressure forces, inertial effects, and bearing clearances. These phenomena significantly influence pump performance, particularly in high-pressure operating conditions. A major contribution in this field is provided in [3], where the effect of radial micromotion of the gears is investigated. Under operating conditions, pressure forces acting on the gear surfaces generate resultant loads that cause small displacements of the gear centers relative to their nominal positions. This radial displacement can be expressed in simplified form as:

$$\delta_r = \frac{F_p}{k_{eq}} \tag{2.11}$$

where:

- F_p is the resultant hydraulic force acting on the gear
- k_{eq} is the equivalent stiffness of the supporting structure

Although the magnitude of δ_r is typically small, its impact on the pump behaviour is significant. In particular, the displacement alters the clearances between mating components, which directly affects leakage flows.

The variation of leakage due to micromotion can be qualitatively expressed as:

$$Q_{leak} = f(h(t), \Delta p) \tag{2.12}$$

where:

- $h(t)$ represents the instantaneous clearance height, varying during operation due to mechanical displacements
- Δp is the pressure difference across the leakage path

As demonstrated in [3], the interaction between hydraulic forces and mechanical compliance generates a strongly coupled fluid-structure behaviour. In particular, the study shows that:

- leakage paths continuously evolve during the operating cycle
- pressure distribution inside the pump chambers is modified by gear displacement
- volumetric efficiency becomes dependent on the elastic behaviour of the mechanical structure

- local pressure peaks and flow ripple may be amplified by dynamic clearance variations

These effects cannot be captured by purely geometric or kinematic models, which assume fixed clearances and perfectly rigid bodies. Consequently, advanced numerical approaches often combine hydraulic models with simplified structural formulations in order to improve prediction accuracy. Besides radial micro-motion, additional mechanical phenomena may contribute to deviations from ideal pump behaviour. Among the most relevant effects are:

- shaft bending and torsional deformation
- elastic deformation of the casing under pressure loading
- bearing compliance and eccentricity
- manufacturing tolerances and assembly inaccuracies
- thermal expansion of rotating and stationary components

All these factors contribute to modifying the instantaneous geometry of the pump during operation and therefore influence pressure generation, leakage losses, volumetric efficiency, and flow ripple characteristics. In high-fidelity simulation environments, these phenomena are sometimes modelled through coupled fluid-structure interaction (FSI) approaches or through lumped compliance models integrated within the hydraulic solver. However, such methods require detailed material properties, accurate boundary conditions, and considerably higher computational effort.

2.6 Gear Profile Design and Geometric Optimization

The performance of crescent-type internal gear pumps is strongly influenced by the geometric characteristics of the rotating and stationary components. Parameters such as tooth profile geometry, radial and axial clearances, gear eccentricity, and crescent separator configuration directly affect volumetric efficiency, leakage phenomena, pressure ripple, and overall hydraulic performance. For this reason, several studies available in the literature have focused on the optimization of these geometric features in order to improve pump efficiency and operating stability. A significant contribution in this field is presented in [4], where the design of optimized rotor profiles for internal gear pumps is investigated with the objective of improving fuel efficiency in automotive lubrication systems. The study demonstrates that modifications of the tooth geometry can substantially reduce internal leakage flows and improve the smoothness of the instantaneous flow rate. In particular, optimized rotor profiles allow a more gradual variation of the trapped chamber volume during gear meshing, reducing flow pulsations and pressure oscillations. As a consequence, the pump exhibits improved volumetric efficiency, lower hydraulic losses, and reduced noise generation. The optimization of the tooth profile is particularly important in internal gear pumps because the instantaneous chamber volume depends directly on the conjugate geometry between the internal and external gears. Even small deviations in the involute profile may significantly modify the local pressure distribution and the leakage paths between adjacent chambers. Therefore, accurate geometric design is essential not only for hydraulic efficiency, but also for ensuring stable meshing conditions and minimizing wear phenomena. In addition to rotor geometry, recent studies have highlighted the fundamental role of the crescent separator. Traditionally considered as a passive sealing element, the crescent plate actively contributes to pressure balancing and leakage compensation within the pump. This aspect is extensively investigated in [6], where a novel separable crescent plate for high-pressure internal meshing gear pumps is proposed and experimentally validated. The authors demonstrate that the geometry of the crescent separator strongly influences the pressure distribution in the transition zone between suction and delivery chambers. In the proposed model, the transition-zone pressure is described through nonlinear differential equations derived from fluid continuity and leakage flow equations. Both radial and axial leakage flows are considered, confirming that even very small variations in clearance dimensions can significantly alter pump performance. The study further shows that the crescent geometry directly affects the balance between hydraulic compensation forces and mechanical contact forces acting on the sealing components. Through constrained optimization procedures implemented in MATLAB, the optimal compensation chamber angle is identified in order to maximize volumetric efficiency while preventing excessive friction and wear.

2.7 Flow Ripple and Noise Generation

Although crescent pumps are often considered relatively smooth-running machines, the flow they generate is inherently affected by periodic oscillations. This phenomenon, commonly referred to as flow ripple, originates from the discrete nature of the inter-tooth chambers and their cyclic volume variation during rotation. From a theoretical perspective, the instantaneous flow rate can be decomposed into a mean component and an oscillating term:

$$Q(t) = Q_{avg} + \tilde{Q}(t) \tag{2.13}$$

where Q_{avg} represents the average flow rate over one revolution, and $\tilde{Q}(t)$ is a periodic function describing the flow fluctuations. The origin of flow ripple lies in the fact that the number of active chambers and their instantaneous volumes vary continuously with the angular position of the gears. As a result, even in ideal conditions without leakage, the flow rate is not perfectly constant. A detailed theoretical analysis of this phenomenon is presented in [7], where the flow ripple in tandem crescent pumps is investigated. This work demonstrates that the amplitude of flow oscillations depends on several geometric and kinematic parameters, including:

- the number of teeth of the gears
- the angular spacing between consecutive chambers
- the relative phase shift between multiple pumping units

One of the most effective strategies to reduce flow ripple consists in employing multiple pumping elements arranged with a phase offset. In this configuration, the total flow rate can be expressed as the superposition of individual contributions:

$$Q_{tot}(t) = Q_1(t) + Q_2(t + \phi) \tag{2.14}$$

where ϕ is the phase shift between the two units. By properly selecting this parameter, it is possible to achieve partial cancellation of the oscillating components. From a practical standpoint, flow ripple is directly related to noise, vibration, and harshness (NVH) issues, which are particularly critical in automotive applications. For this reason, its accurate prediction and mitigation represent key objectives in pump design.

In the context of analytical models, flow ripple emerges naturally from the periodic variation of chamber volumes, as described in [2]. However, its amplitude in real machines is also influenced by leakage, compressibility, and structural compliance, which are not captured by purely geometric formulations.

2.8 Trapped Oil Phenomena and Pressure Peaks

A critical phenomenon in crescent pumps is the formation of trapped fluid volumes during the meshing process. These volumes occur when a portion of fluid becomes temporarily enclosed between adjacent teeth, without a direct connection to either the suction or delivery ports.
As the gears continue to rotate, the trapped volume is subjected to compression due to the decreasing space between the teeth. Since the trapped mass of fluid is approximately conserved over this short interval, the reduction of the control volume produces a rapid pressure increase inside the trapped chamber. The pressure evolution can be related to the compressibility of the fluid through the definition of the bulk modulus:

$$K = -V\frac{dp}{dV} \tag{2.15}$$

where K is the bulk modulus of the fluid, V is the instantaneous trapped volume, and p is the fluid pressure. Assuming a constant bulk modulus, negligible leakage, and quasi-static compression of the trapped fluid, the ***Equation 2.15*** can be rearranged as:

$$dp = -K\frac{dV}{V} \tag{2.16}$$

Integrating between the initial condition $(p_0, V_0)$and the instantaneous condition $(p(t), V(t))$:

$$\int_{p_0}^{p(t)} dp = -K\int_{V_0}^{V(t)} \frac{dV}{V} \tag{2.17}$$

which yields:

$$p(t) - p_0 = -K\ln\left(\frac{V(t)}{V_0}\right) \tag{2.18}$$

or equivalently:

$$p(t) = p_0 + K\ln\left(\frac{V_0}{V(t)}\right) \tag{2.19}$$

where p_0 is the initial pressure of the trapped fluid, V_0 is the initial trapped volume, and $V(t)$ is the instantaneous trapped volume during meshing. The ***Equation 2.19*** highlights the strong sensitivity of pressure to volume reduction. Even relatively small decreases in trapped volume may generate significant pressure peaks because of the high bulk modulus of hydraulic fluids. The consequences of this phenomenon are significant for generation of high-pressure peaks, increasing mechanical stress on components and contribution to noise and vibration. The study presented in [5] provides a detailed numerical analysis of trapped oil pressure evolution. Their results confirm that the magnitude of pressure peaks strongly depends on the rate of volume reduction and on the compressibility of the fluid. To mitigate these effects, practical design solutions are commonly adopted and one of the most effective approaches consists in the introduction of relief grooves, which provide a controlled path for fluid escape, thereby reducing pressure build-up. Despite their importance, trapped volume effects are not included in standard analytical flow rate models, which assume continuous communication between chambers and ports. As a result, they represent a key source of discrepancy between theoretical predictions and real pump behaviour.

2.9 Relations to the Present Thesis

The literature reviewed in the previous sections highlights the progressive evolution of crescent pump modelling approaches, ranging from purely analytical formulations to lumped parameter methods and fully coupled numerical simulations. Each modelling strategy provides a different level of accuracy and physical detail, depending on the phenomena considered. In the present thesis, the main focus is placed on the reverse engineering and geometric reconstruction of the pump, since the geometric characterization of the machine directly affects the accuracy of the analytical flow rate prediction. The developed model is therefore primarily based on analytical and geometric formulations, using parameters extracted from CAD models reconstructed through reverse engineering procedures. This approach allows the theoretical flow rate and the volumetric evolution of the inter-tooth chambers to be evaluated as functions of the gear geometry and rotational position. Although the implemented formulation is mainly devoted to the geometric and volumetric analysis of the pump, the literature demonstrates that several additional physical phenomena contribute to the deviation between theoretical predictions and real operating behaviour. In particular, leakage flows, pressure dynamics, fluid compressibility, trapped oil effects, and mechanical deformations significantly influence the actual pump performance, especially under high-pressure operating conditions. A complete lumped parameter implementation has not been developed within the scope of this work. Nevertheless, the analysis of the available models provides important insight into the physical mechanisms governing real crescent pumps and clarifies the limitations of purely theoretical formulations. Similarly, mechanical compliance and gear micro-motion are not explicitly included in the implemented model, although their influence is acknowledged as one of the possible causes of discrepancies between calculated results and the experimental performance data provided by the manufacturer. For the same reason, trapped oil phenomena are not directly modelled, but their potential influence is considered when interpreting differences between theoretical and experimental results. Consequently, the analytical model developed in this thesis should be regarded as an upper-bound representation of the pump performance, while real operating conditions inevitably lead to lower efficiency values due to the combined action of hydraulic, mechanical, and tribological effects. Overall, the reviewed literature establishes the theoretical framework necessary to interpret the results obtained in this work and identifies the intermediate position of the adopted methodology between simplified geometric models and more advanced multi-physics simulations.

3. Pump Description and Technical Specifications

3.1 Pump Main Specifications

The hydraulic machine analysed in this work, shown in ***Figure 3.1***, is an internal gear pump manufactured by Bosch Rexroth, identified by the material number R900932265. According to the manufacturer datasheet, the pump belongs to the PGF series and corresponds to the model PGF2-2X/006 R E 01VE4, characterized by a fixed geometric displacement.

Figure 3.1 - Bosch Rexroth R900932265

Starting from the pump serial number, we can extract from the manufacture datasheet shown in ***Figure 3.2*** the main technical specifications summarized below:

- Geometric displacement: $V_g = 6.5\ \frac{\text{cm}^3}{rev}$
- Nominal flow rate: $Q = 9.4\ \frac{l}{min}$ at 1450 rpm
- Minimum rotational speed: 600 rpm
- Maximum rotational speed: 3600 rpm
- Continuous operating pressure: 210 bar
- Maximum intermittent pressure: 250 bar

These data are used as reference values for the validation of the geometric and volumetric analysis developed in this work.

Dimensions [mm]

Internal gear pump | PGF Series 2X and 3X 15

Dimensions frame size 2

Parallel keyed shaft, DIN 6885, with through drive

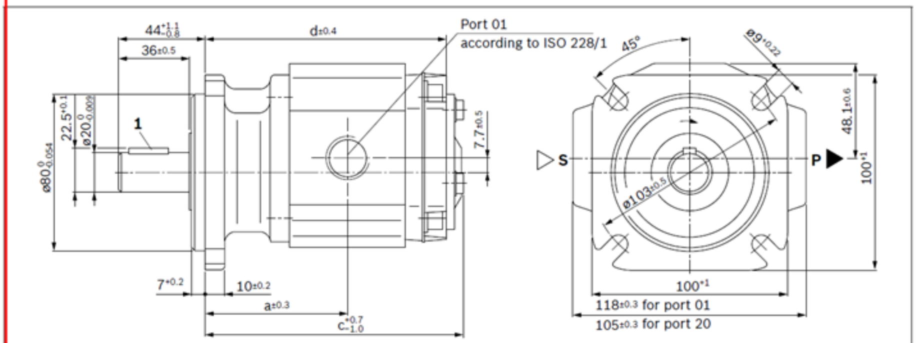

1 Shaft key B6 × 6 × 25

Type				Material numbers	a	c	d	Port standard	Port optional
PGF2-2X/	**006**	R	**E** 01VE4	R900932265	63	115.2	104.1	01	20
	008	R	**E** 01VE4	R900932266	64.8	118.7	107.6	01	20
	011	R	**E** 01VE4	R900932271	67.5	124.2	113.1	01	20
	013	R	**E** 20VE4	R900943181	70	129.2	118.1	20	01
	016	R	**E** 20VE4	R900932193	72.5	134.2	123.1	20	01
	019	R	**E** 20VE4	R900943182	75.5	140.2	129.1	20	01
	022	R	**E** 20VE4	R900932126	78.5	146.2	135.1	20	–

Frame size			**BS**	**2**	**2**	**2**	**2**	**2**	**2**	**2**
Size			NG	6.3	8	11	13	16	19	22
Displacement, geometric		V_g	cm^3	6.5	8.2	11	13.3	16	18.9	22
Input speed		n_{min}	rpm	600	600	600	600	600	600	600
		n_{max}	rpm	3600	3600	3600	3600	3600	3600	3000
Operating pressure, absolute										
Inlet		p	bar	0.6 to 3	0.6 to 3	0.6 to 3	0.6 to 3	0.6 to 3	0.6 to 3	0.6 to 3
Outlet	continuous	p_N	bar	210	210	210	210	210	210	180
	intermittend[1)]	p_{max}	bar	250	250	250	250	250	250	210
Flow (at n = 1450 rpm, p = 10 bar, ν = 30 mm^2/s)		q_V	l/min	9.4	11.9	16	19.3	23.3	27.4	31.9
Power consumption Minimum required Drive power (at p = 1 bar)		P_{input}	kW	0.75	0.75	0.75	0.75	0.75	1.1	1.1
Moment of inertia (around drive axis)		J	kgm^2	0.000074	0.000090	0.00012	0.00014	0.00016	0.00019	0.00022
Weight[2)]		m	kg	2.1	2.2	2.4	2.6	2.7	2.9	3.1
Shaft loading				Radial and axial forces (e.g., belt pulley) only after consultation						
Type of mounting				Flange mounting						

Figure 3.2 – Pump main specification

3.2 Pump Functional Overview

This specific hydraulic pump is a leak-gap-compensated internal gear pump with a fixed displacement. As we can see in ***Figure 3.3***, it consists basically of housing (1), bearing cover (1.1), cover (1.2), ring gear (2), pinion shaft (3), slide bearings (4), axial discs (5) and stop pin (6). Moreover, as we can see in ***Figure 3.4***, the segment assembly (7) is composed by a segment (7.1), a segment carrier (7.2) and the sealing rolls (7.3).

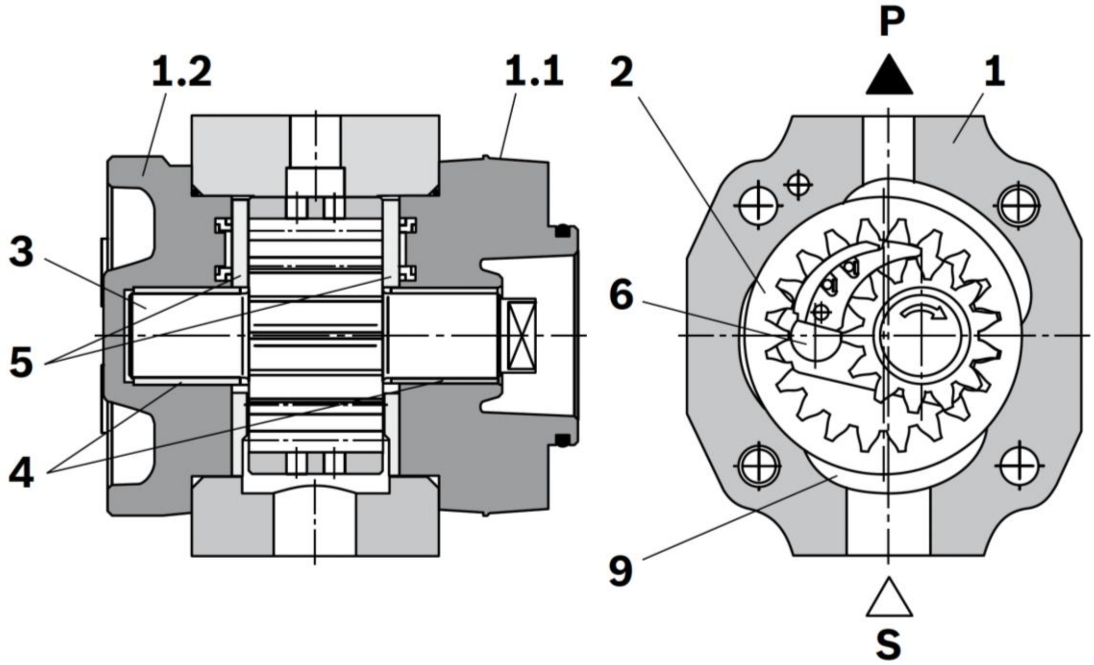

Figure 3.3 – Pump main components

The hydrodynamically supported pinion shaft (3) drives the internally toothed ring gear (2) according to the rotation direction illustrated in ***Figure 3.4***. As the gears rotate, the chamber volume progressively increases within the suction region over an angular extension of approximately 180°, generating a pressure drop that allows the fluid to enter the pumping chambers. The sickle-shaped separator assembly (7), visible in ***Figure 3.4***, provides the hydraulic separation between the suction and delivery zones. In the delivery region, the teeth of the pinion shaft (3) progressively mesh with the tooth spaces of the ring gear (2), causing the trapped fluid to be displaced toward the pressure port (P).

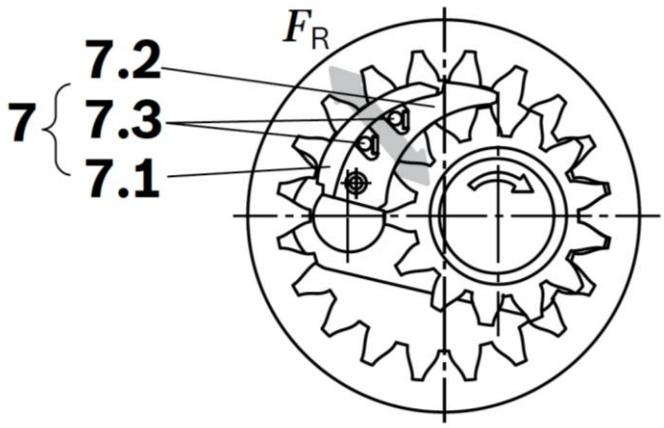

Figure 3.4 – Radial compensation force, segment assembly

As illustrated in ***Figure 3.4***, the radial compensation force acts on both the segment (7.1) and the segment carrier (7.2). The geometry of the area ratios, together with the positioning of the sealing rolls (7.3) located between the segment and the segment carrier, is specifically designed to achieve an almost gap-free sealing condition between the ring gear (2), the segment assembly (7), and the pinion shaft (3). In addition, spring elements placed beneath the sealing rolls (7.3) maintain sufficient contact pressure even under very low operating pressures. As shown in ***Figure 3.5***, the axial compensation force is generated within the pressure chamber by the pressure field acting on the compensation zones (8) of the axial discs (5). Consequently, the axial clearances between the rotating and stationary components are minimized, ensuring highly effective axial sealing of the pressure chamber.

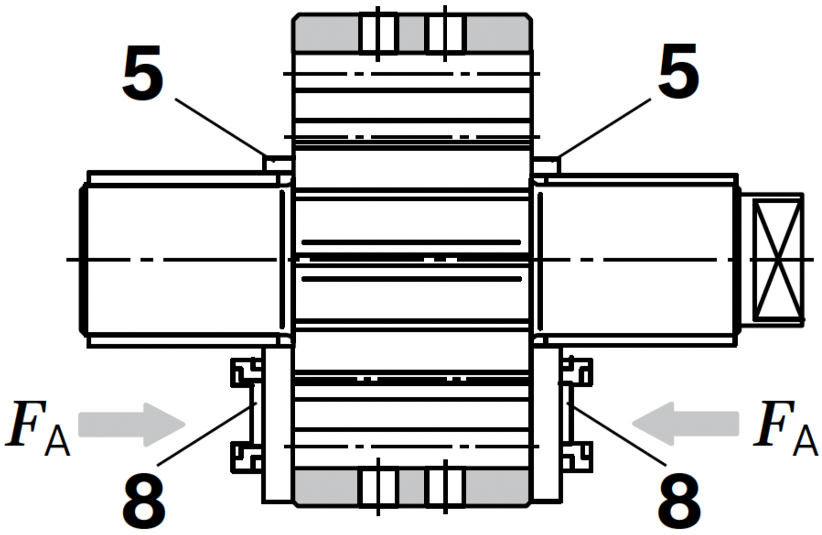

Figure 3.5 – Axial compensation force

4. Reverse Engineering and Parameters Identification

4.1 Data Acquisition and Measurement Tools

Before starting the geometrical reconstruction and the theoretical analysis of the crescent internal gear pump, a preliminary preparation phase is required. This phase is fundamental because the quality of the final CAD model and of the analytical results strongly depends on the accuracy of the acquired geometrical data. The purpose of the preliminary procedure is therefore to safely disassemble the pump, identify all the functional components and finally, clean and prepare the parts for measurements as shown in ***Figure 4.1***.

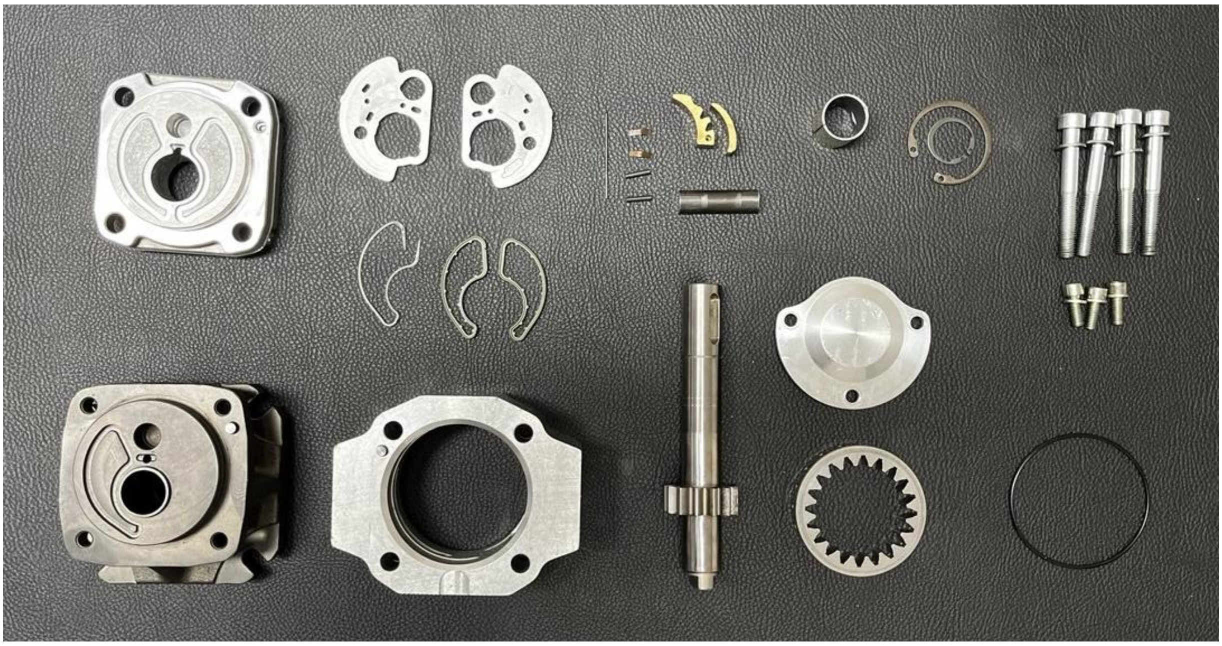

Figure 4.1 – Disassembled pump

The main measurement tool used was a vernier caliper shown in ***Figure 4.2***, which allowed the acquisition of the main geometric dimensions with sufficient accuracy for the purposes of the analysis. These main measured quantities include external dimensions of housings, gear outer and inner diameters, gear width, dimensions of accessible internal and external features.

Figure 4.2 – Digital vernier caliper

Certain components, including the compensation plates, the crescent element, and the gears teeth profiles, are characterized by complex geometries that are not easily accessible for direct measurement using a vernier caliper. For this reason, a complementary approach based on two-dimensional scanning was employed to capture their geometric features.

4.2 CAD Modelling of the Pump Assembly

The 3D model of the entire assembly shown in Figure was developed in SolidWorks, a parametric CAD software widely used in mechanical engineering. In ***Figure 4.3*** we can see the entire pump assembly in SolidWorks environment.

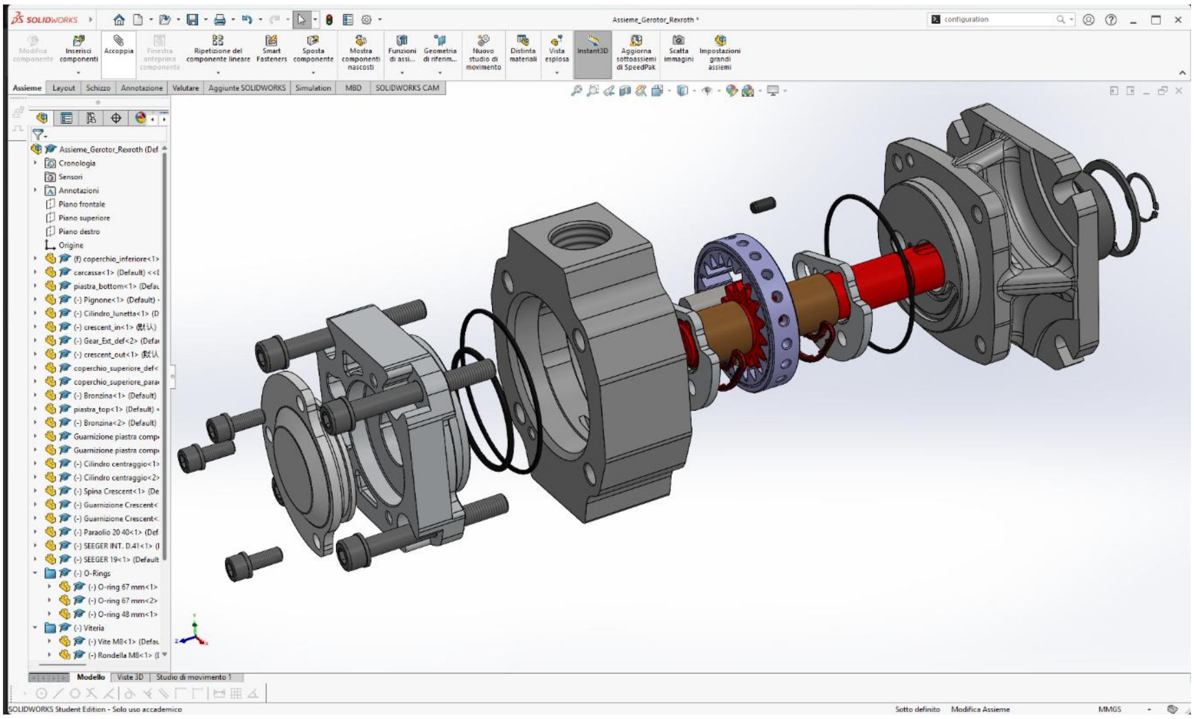

Figure 4.3 – Pump assembly in SolidWorks environment

As said before, simple components such as housings, bearings, screws and so on, were modelled starting from the measurements, using a classic 3D parametric modelling workflow.

4.2.1 Pump Housing

A main component worth describing is the pump housing. It encloses all internal components and provides the structural support of the system. It defines the internal fluid domains and integrates the inlet and outlet ports. Its geometry directly influences the flow path and the evolution of the fluid volumes within the pump. It was modelled based on the measured external dimensions and the general layout provided by the datasheet.
In ***Figure 4.4*** we can see the detailed model of the entire pump housing which includes the main housing, the bearing covers and the external cover.

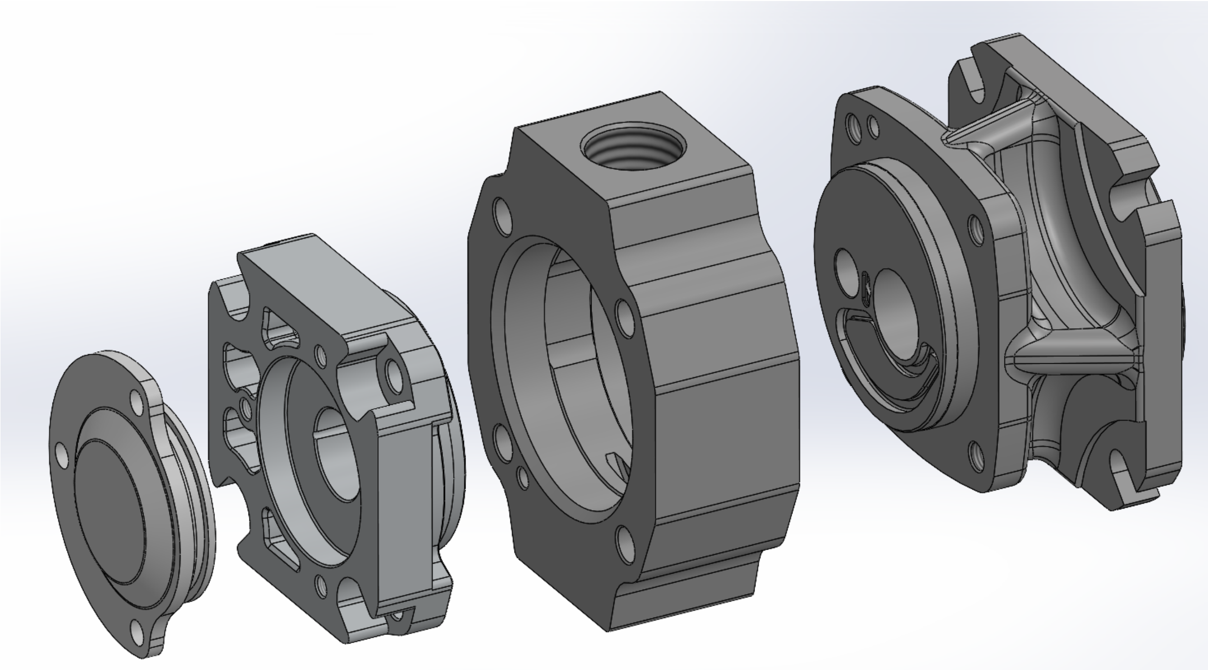

Figure 4.4 – Pump housing assembly

4.2.2 Compensation Plates and Plates Gaskets

Conversely, some components, including the compensation plates, the crescent element, and the gears teeth profiles, are characterized by complex geometries that are not easily accessible for direct measurement using a vernier caliper. For this reason, a complementary approach based on two-dimensional scanning was employed to capture their geometric features. In ***Figure 4.5*** we can see the scan of the compensation plate that cannot be modelled through direct measurements. Once the scan is imported in the CAD software, the modelling is performed and all the measurements are obtained as shown in ***Figure 4.6***. The plate gaskets are directly derived from the geometry of the housing as shown in ***Figure 4.7***.

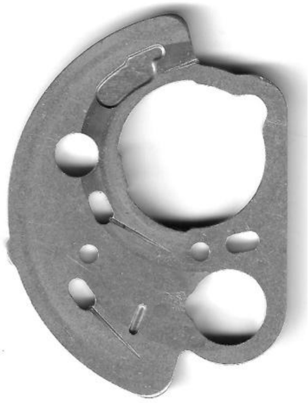

Figure 4.5 – 2D scan of crescent element, ring gear and compensation plate

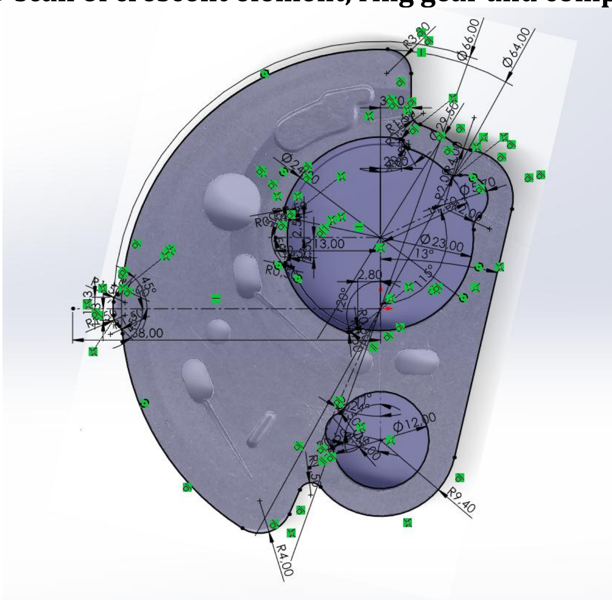

Figure 4.6 – 2D scan-based modelling

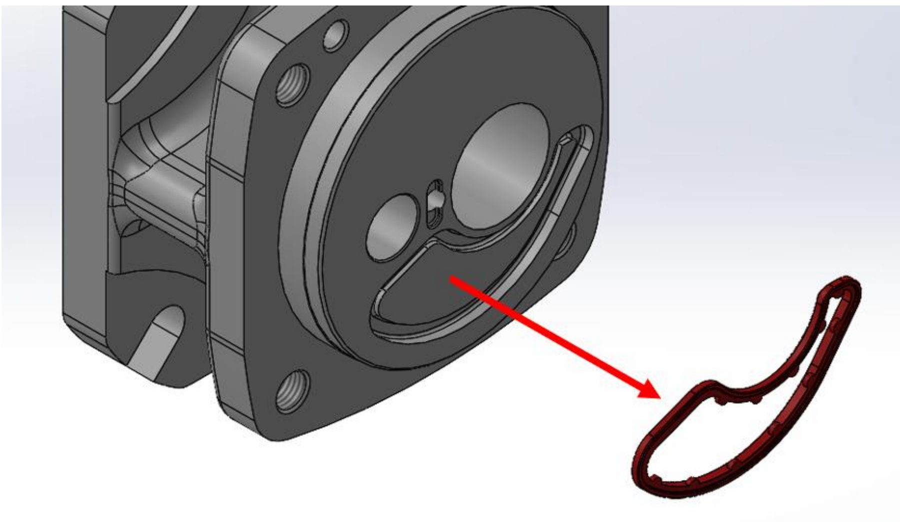

Figure 4.7 – Compensation plates gasket

4.2.3 Crescent Elements

The same approach used for the compensation plates is used for the crescent elements so a two-dimensional scanning is imported in the Solidworks environment to capture the geometric features and measures. Then a 2D scan-based modelling shown in **Figure 4.8** is performed in order to model the crescent geometry shown in ***Figure 4.9***.

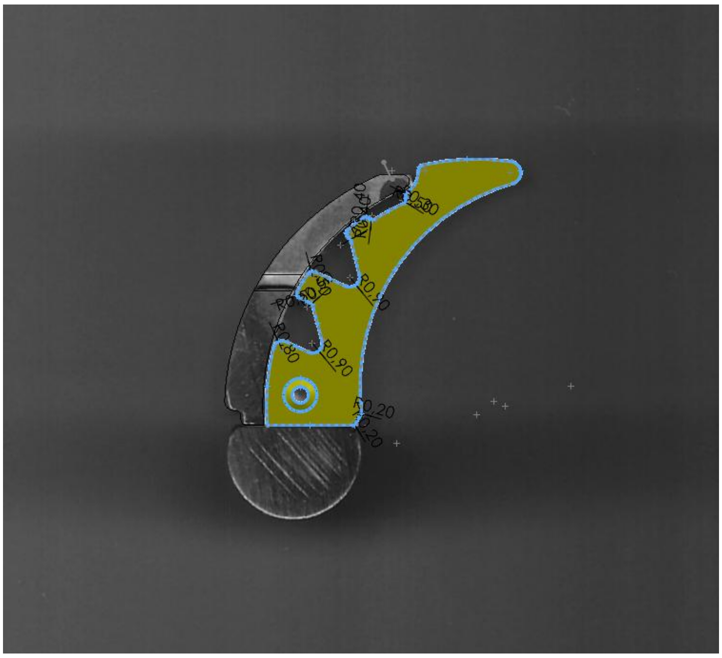

Figure 4.8 – Crescent element

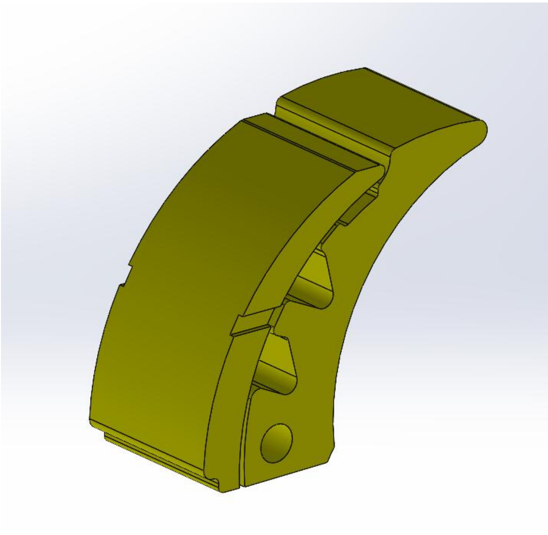

Figure 4.9 – crescent 3D model

4.2.4 Internal Gearset

The reconstructed geometry provides a detailed representation of the pump components, but it does not directly supply the analytical parameters required to describe the pump performance that is mainly influenced by the internal gear meshing shown in ***Figure 4.10***.

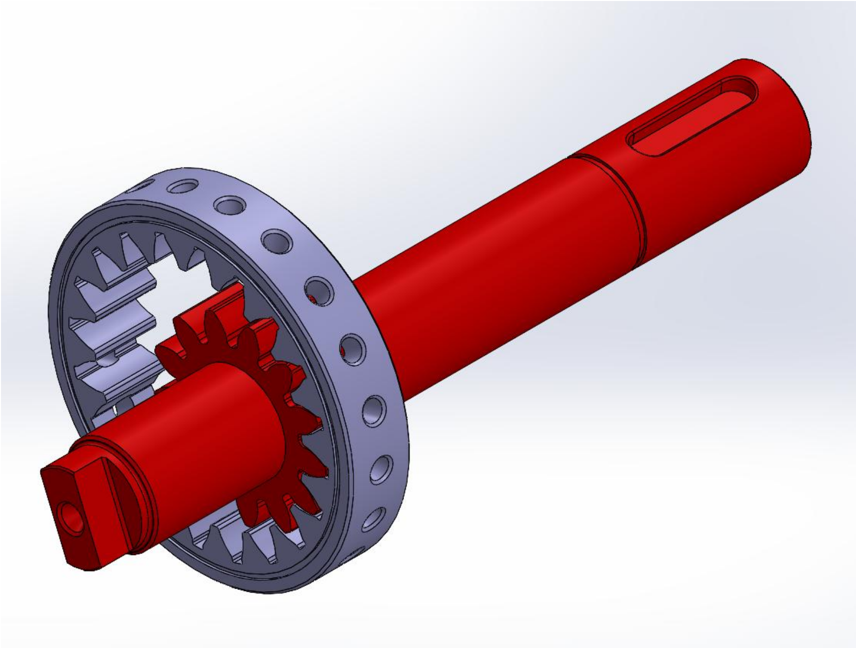

Figure 4.10 – Pinion and ring gear

Therefore, a parameter identification procedure was carried out in order to estimate the main geometric quantities of the gear set.

The number of teeth of the pinion and ring gear was directly determined from the model:

Ring gear tooth number: $z_r = 20$
Pinion tooth number: $z_p = 13$

The center distance between the gears was directly measured:

$$I_g = 8.8\, mm$$

The axial width of the gears was also measured:

$$b = 13 \text{ mm}$$

The cutting module of the gear set was estimated using the geometric relation associated with internal gear meshing:

$$m_0 = \frac{2I_g}{z_r - z_p} \tag{4.1}$$

The cutting pitch radius of the pinion is:

$$R_{p0} = \frac{N_d m_0}{2} \tag{4.2}$$

while for the ring gear:

$$R_{p02} = \frac{N_{d2} m_0}{2} \tag{4.3}$$

These radii correspond to the nominal generating geometry of the gears. However, in the actual operating condition, the pressure angle is modified by the real center distance. At this point we can hypothesize a pressure angle and then validate it by comparing the involute with the 2D scan of the ring gear. The chosen value of pressure angle is $\theta_0 = 25°$. Therefore, the working pressure angle must be determined using the following formulation:

$$\theta_k = \arccos\left(\frac{R_{p02} - R_{p0}}{I_k}\cos(\theta_0)\right) \tag{4.4}$$

This expression reflects the fact that the kinematics of meshing are controlled by the actual center distance between the gears, not only by the nominal cutting geometry. Once θ_k is known, the working pitch radius of the pinion can be obtained:

$$R_{pl} = \frac{R_{p0}\cos(\theta_0)}{\cos(\theta_k)} \tag{4.5}$$

and for the ring gear:

$$R_{pl2} = \frac{R_{p02}\cos(\theta_0)}{\cos(\theta_k)} \tag{4.6}$$

These radii are the effective rolling radii associated with the operating meshing condition. They play a central role in relating angular motion to the geometrical evolution of the fluid chambers. The base circle radius of the pinion is instead written as:

$$\rho = R_{p0}\cos\theta_0 \tag{4.7}$$

and the base circle radius of the ring gear:

$$\rho_2 = R_{p02}\cos\theta_0 \tag{4.8}$$

In order to validate the gear geometry, the profile of a single tooth was extracted from the 2D scan of the ring gear and the scanned profile was then compared with the theoretical involute curve shown in ***Figure 4.11***. Starting from the values of the base circle radius found before, the parametric equation of the involute was implemented in Solidworks:

$$x = \rho_2 \cdot \big(cos(t) + t \cdot sin(t)\big) \cdot cos(-2\rho_2) - \rho_2 \cdot (sin(t) - t \cdot cos(t)) \cdot sin(-2\rho_2) \quad (4.9)$$

$$y = \rho_2 \cdot (cos(t) + t \cdot sin(t)) \cdot sin(-2\rho_2) + \rho_2 \cdot (sin(t) - t \cdot cos(t)) * cos(-2\rho_2) \quad (4.10)$$

where ρ_2 is the base circle radius of the ring gear involute.

As shown in ***Figure 4.11***, we have a match between the 2D scan and the parametric involute curve so we can consider a working angle $\theta_0 = 25°$ plausible.

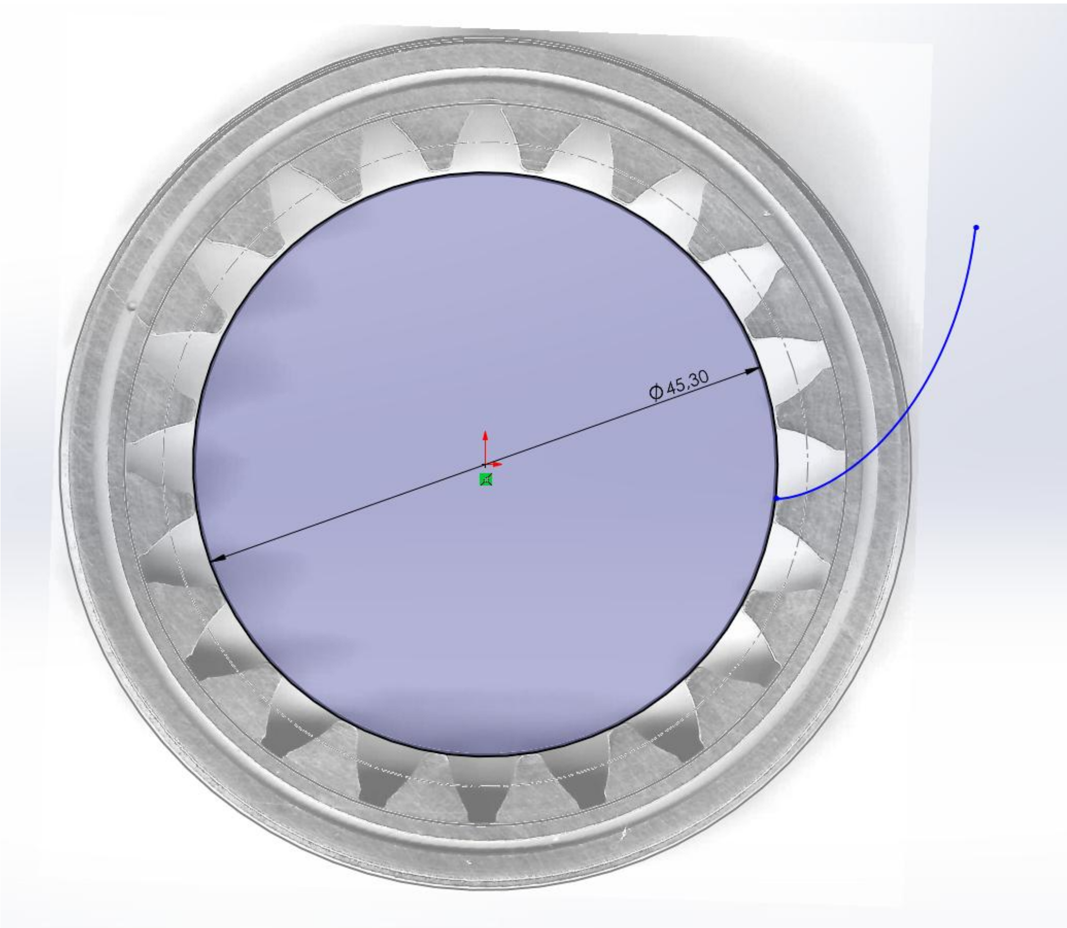

Figure 4.11 – Involute parametric curve of the ring teeth

The same approach is then applied for the pinion gear but in this case we can not compare the cad geometry with a 2D scan because of the pinion geometry itself, but we can implement the same parametric equation in Solidworks as shown in ***Figure 4.12***:

$$x = \rho \cdot \big(cos(t) + t \cdot sin(t)\big) \cdot cos(-2\rho) - \rho \cdot (sin(t) - t \cdot cos(t)) \cdot sin(-2\rho) \qquad (4.11)$$

$$y = \rho \cdot (cos(t) + t \cdot sin(t)) \cdot sin(-2\rho) + \rho \cdot (sin(t) - t \cdot cos(t)) * cos(-2\rho) \qquad (4.12)$$

where ρ is the base circle radius of the pinion involute.

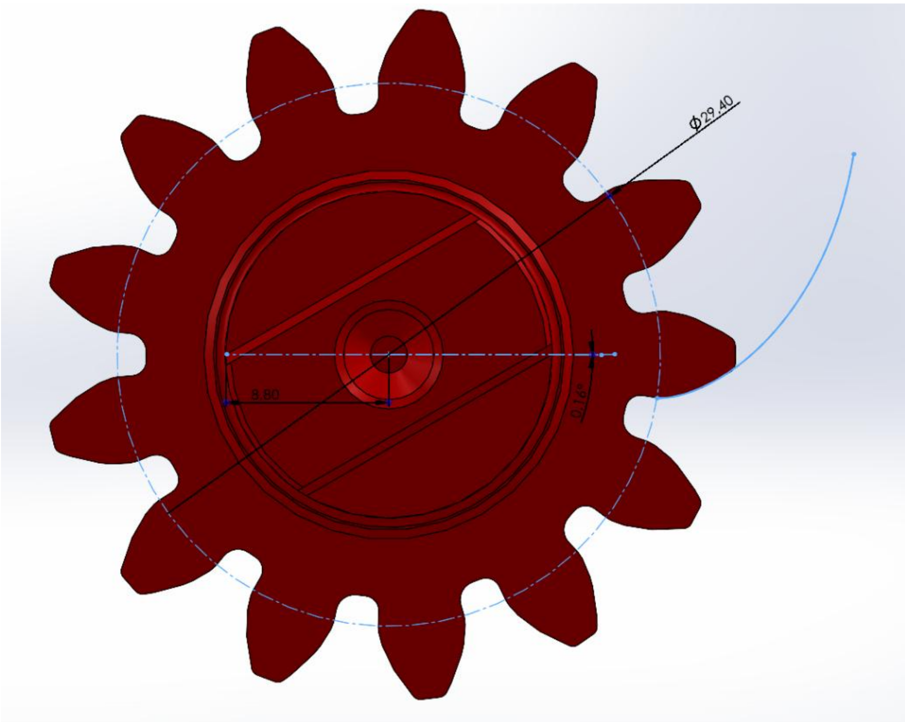

Figure 4.12 – Involute parametric curve of the pinion teeth

For sake of completeness, all the found values with reference of the internal gears meshing are listed in ***Table 4.1***.

Parameter	Parameter description	Value
z_r	Ring gear tooth number	20
z_p	Pinion tooth number	13
m_0	Cutting module of the gear set	2.5 mm
I_g	Center distance between the gears	8.80 mm
b	Axial width of the gears	13 mm
θ_0	Pressure angle	25º
θ_k	Working pressure angle	25.67º
R_{p0}	Cutting pitch radius of the pinion	16.3 mm
R_{p02}	Cutting pitch radius of the ring gear	25 mm
R_{pl}	Working pitch radius of the pinion	16.3 mm
R_{pl2}	Working pitch radius of the ring gear	25.1 mm
ρ	Base circle radius of the pinion	14.7 mm
ρ_2	Base circle radius of the ring gear	22.7 mm

Table 4.1 – Internal gear meshing parameters

5. Performance Evaluation

The performance of an internal gear pump is strongly influenced by the geometry of the meshing gear pair, since the volumetric displacement mechanism is directly related to the evolution of the inter-tooth chambers during shaft rotation. Starting from the reverse-engineered CAD model of the pump, an analytical formulation was implemented in MATLAB in order to estimate the main volumetric quantities of interest, namely the theoretical displacement, the instantaneous and average theoretical flow rate, the trapped volume evolution, and a simplified estimation of axial leakage losses. The purpose of the model is not to reproduce the full detail of the original simulation environment, but rather to provide a compact and physically consistent analytical tool capable of linking the measured geometry of the real pump to the theoretical framework of gear pump kinematics. In this sense, the model may be interpreted as an equivalent analytical reconstruction of the actual gear set, based on the main geometrical parameters identified from CAD measurements and organized according to the analytical approach proposed in [9]. In the present case, the gear unit is an internal gear set, therefore the analytical formulation has been specialized accordingly. The implementation was developed as a MATLAB script, in which the various computational steps follow the same logical sequence adopted in the analytical derivation: definition of the input data, evaluation of the principal geometrical quantities, reconstruction of chamber volumes, computation of the volume derivatives, determination of the theoretical flow rate, and finally estimation of volumetric losses.

5.1 Input Parameters

The analytical model starts from a set of geometrical quantities presented in the previous chapter and derived from reverse engineering. The parameters used in the MATLAB implementation are listed below:

- number of teeth of the pinion: $z_p = 13$;
- number of teeth of the driven ring gear: $z_r = 20$;
- imposed centre distance: $I_g = 8.8$ mm;
- normal module: $m_0 = 2.5$ mm;
- normal pressure angle: $\theta_0 = 25°$;
- addendum radius of the driver gear: $R_e = 18.75$ mm;
- root radius of the driver gear: $R_{f0} = 13.3$ mm;
- outer radius of the internal gear: $R_{e2} = 28.0$ mm;
- inner radius of the internal gear: $R_{f2} = 22.5$ mm;
- external housing radius associated with the ring gear seat: $R_{ext} = 33.0$ mm;
- gear width: $b = 13$ mm;
- normal backlash between teeth: $h_{sn} = 0.2$ mm.

Additional parameters are introduced in order to preserve consistency with the analytical structure of the reference formulation, including tool addendum and dedendum coefficients, shaper coefficients, axial clearance, radial clearance, suction and delivery angular timing, and the geometrical dimensions of the supporting pins. These values do not all arise directly from measurement; some of them are introduced as modelling parameters required to define an equivalent analytical representation of the real machine.[3]

Firstly, we can calculate the angular pitch of the two gears:

$$\Delta\phi = \frac{2\pi}{z_p} \tag{5.1}$$

$$\Delta\phi_2 = \frac{2\pi}{z_r} \tag{5.2}$$

The periodicity of the machine implies that the flow waveform repeats over one pitch of the driving pinion. For this reason, a complete theoretical description can be carried out over the interval:

$$0 \leq \phi \leq \Delta\phi$$

This is exactly the approach implemented in the MATLAB code.

5.2 Active Meshing Segment

As presented in [9], not the whole tooth profile contributes to the useful variation of chamber volume. Instead, only a specific portion of the meshing region is active in defining the opening, closure, and transfer of the fluid chambers.
The first auxiliary quantity is:

$$\mathrm{TT}' = (\rho + \rho_2)\tan\theta_k \tag{5.3}$$

This term represents the total extension of the theoretical contact segment measured along the tangent direction associated with the working pressure angle as shown in ***Figure 5.1***. It may be regarded as a characteristic length governing the transition between the beginning and end of effective meshing.

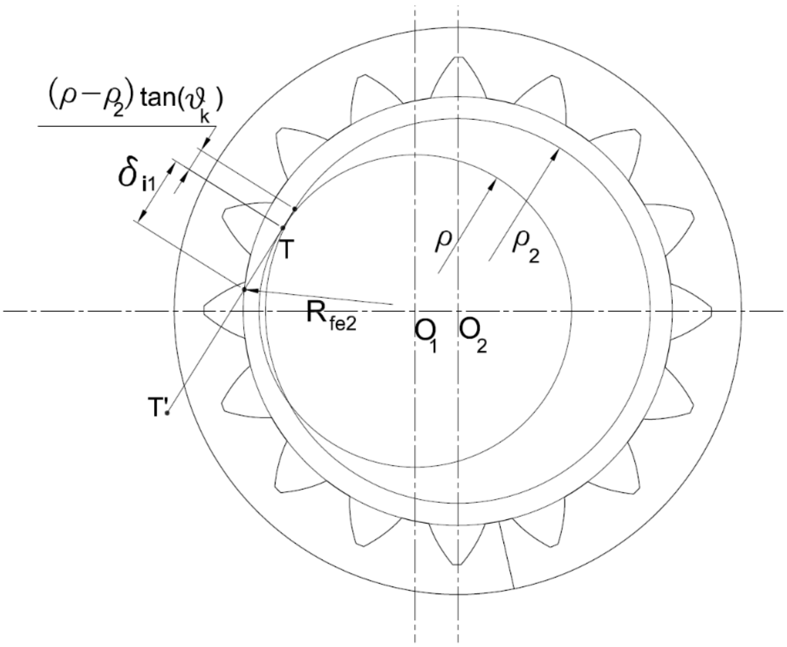

Figure 5.1 – Total extension of the theoretical contact segment

As shown in ***Figure 5.2***, the unused part on the internal gear side is described by:

$$\delta_{i2} = \mathrm{TT'} - \sqrt{R_t^2 - \rho^2} \tag{5.4}$$

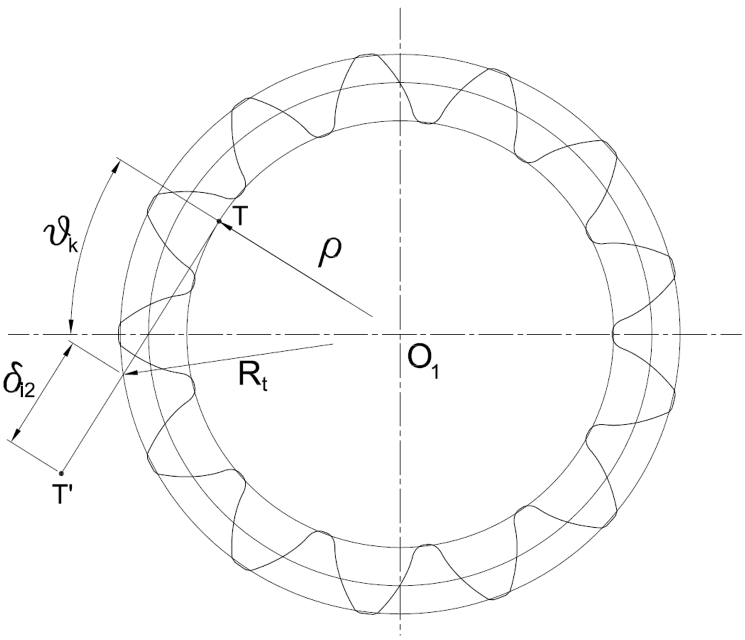

Figure 5.2 – Unused part on the internal gear

The quantity $\sqrt{R_t^2 - \rho^2}$ derives from the geometry of the involute profile. Since the involute can be parametrized as a function of the tangent distance from the base circle, this expression identifies the corresponding tangent coordinate at the end involute radius of the pinion. Similarly, the unused part on the pinion side is:

$$\delta_{i1} = \max\left[\sqrt{R_{fe2}^2 - \rho_2^2} - (\rho_2 - \rho)\tan\theta_k, \sqrt{R_i^2 - \rho^2}\right] \tag{5.5}$$

This expression deserves attention. It is defined as the maximum of two candidate lengths because the actual start of the active profile is constrained by the geometry of both gears. The first term is related to the end involute radius of the internal gear, translated by the offset induced by the difference in base radii. The second term comes from the start involute radius of the pinion. The maximum operator ensures that only the physically admissible active segment is retained. These lengths are not mere geometric corrections. They are essential in establishing the real limits of the fluid chambers and therefore in obtaining the correct volume derivatives.

5.3 Auxiliary Angular Variables

The mathematical model presented in [9] investigates all those properties of the pump that depend solely on the geometry of its constituent elements. To simplify the formulation, auxiliary variables expressed as functions of the angular position of the driving gear will be introduced. Since the analysed quantities are periodic functions, they are normalized with respect to the angular pitch of the driving gear. For the delivery volume, an auxiliary variable is defined with the following properties:

- it varies between 0 and $\Delta\phi$ as ϕ varies from 0 to $+\infty$;
- it is equal to 0 when a new contact between a tooth of the driving gear and a tooth of the driven gear begins, namely when the trapped volume is generated.

The equation relating the auxiliary variable to the angular rotation ϕ of the driving gear is:

$$\nu_m = \left(\left(\frac{\phi + \phi_s}{\Delta\phi}\right) - int\left(\frac{\phi + \phi_s}{\Delta\phi}\right)\right)\Delta\phi \tag{5.6}$$

where ϕ_s is the value assumed by ν_m when the gears are in the reference condition, and therefore represents the rotation that must be imposed on the driving gear in order to move from the instant in which a new contact point P_1^o is generated to the reference condition with the contact point located at P_0 as shown in ***Figure 5.3***. The value of ϕ_s is obtained from the following relation:

$$\phi_s = \tan(\vartheta_k) - \nu_0 + \phi_1' \tag{5.7}$$

In the previous relation, the operating pressure angle of the gear pair appears; the other angles are rotations of the driving gear corresponding to linear distances. In particular, $\nu_0$is the angle corresponding to the unused portion of the line of contact segment (on the side of the driving gear), while ϕ_1' corresponds to the rotation of the driving gear required to move the contact point from the instantaneous center of rotation $C$to point P_0, where the gear is located in the reference condition as shown in ***Figure 5.4***.

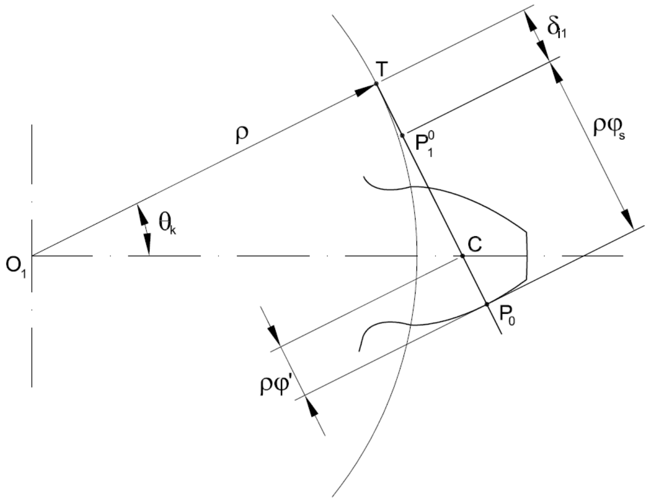

Figure 5.3 – Angular constants

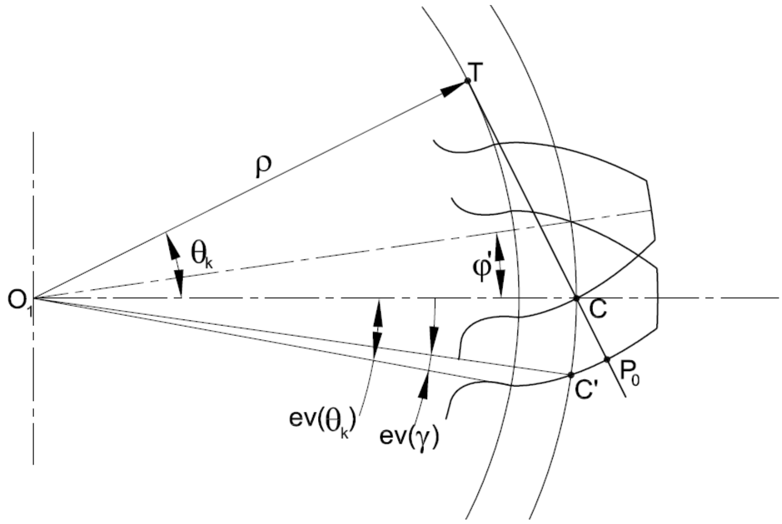

Figure 5.4 – Angular constant ϕ_1'

Starting from the condition in which the contact point is located at C, after a rotation ϕ_1', if the contact point is considered fixed with respect to the gear, it moves to C'.

$$\nu_0 = \frac{\delta_{i1}}{\rho} \tag{5.8}$$

$$\phi_1' = \mathrm{ev}(\vartheta_k) - \mathrm{ev}(\gamma) \tag{5.9}$$

where:

$$\gamma = \operatorname{acos}\left(\frac{\rho}{R_{pl}}\right) \tag{5.10}$$

Geometrically, γ identifies the angular position associated with the working pitch radius when referred to the base circle. Since the involute function links base-circle geometry to actual tooth profile geometry, γ enters naturally into the kinematic phase relations. Once this constant is known, the auxiliary variable ν_m can be plotted as a function of the angular position of the driving gear and the evolution is shown in ***Figure 5.5***. The delivery variable ν_m increases linearly with the rotation angle ϕ, then suddenly returns to zero. This discontinuity is a consequence of the modular definition of the auxiliary variable. In fact, ν_m is defined within one angular pitch and is reset every time a new tooth-pair configuration begins. Therefore, the vertical drop represents the transition from one pitch interval to the following one.

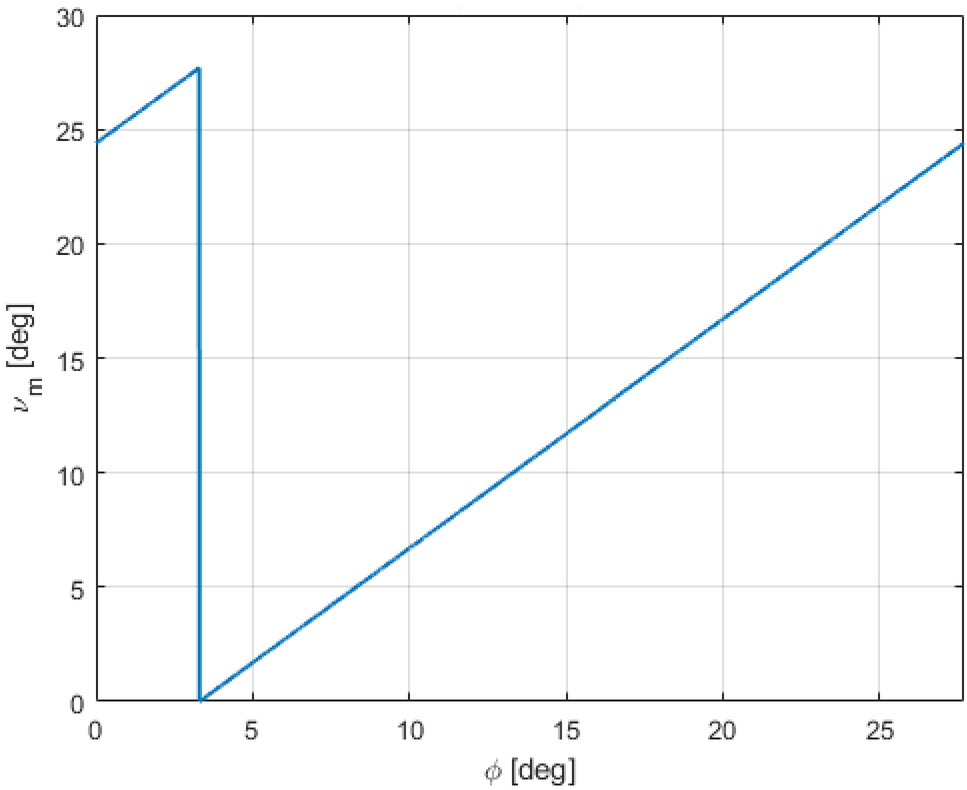

Figure 5.5 – Auxiliary delivery variable plot

For the suction volume, an auxiliary variable $\nu_a$is introduced, completely analogous to the variable ν_m, and defined as a function of the angular rotation $\phi$with the following properties:

- it varies between 0 and $\Delta\phi$ as ϕ varies from 0 to $+\infty$;
- it is equal to 0 when two teeth separate (i.e., when the trapped volume disappears):

$$\nu_a = \left(\left(\frac{\phi + \phi_s'}{\Delta\phi}\right) - int\left(\frac{\phi + \phi_s'}{\Delta\phi}\right)\right)\Delta\phi \tag{5.11}$$

where ϕ_s' is the value assumed by ν_a when the gears are in the reference condition, and therefore represents the rotation that must be imposed on the gear in order to move the contact point P_0 from the reference position to the end of the meshing segment at P_2^o as shown in ***Figure 5.6***.

In this case, the relations are derived along the portion of the line of contact located near the driven gear; therefore, the obtained results must be referred to the rotations of the driving gear through the transmission ratio.

$$\phi_s' = \Delta\phi + \phi_1' - \frac{z_r}{z_p}(\tan(\vartheta_k) + \nu_0') \tag{5.12}$$

where:

$$\nu_0' = \frac{\delta_{i2}}{\rho} \tag{5.13}$$

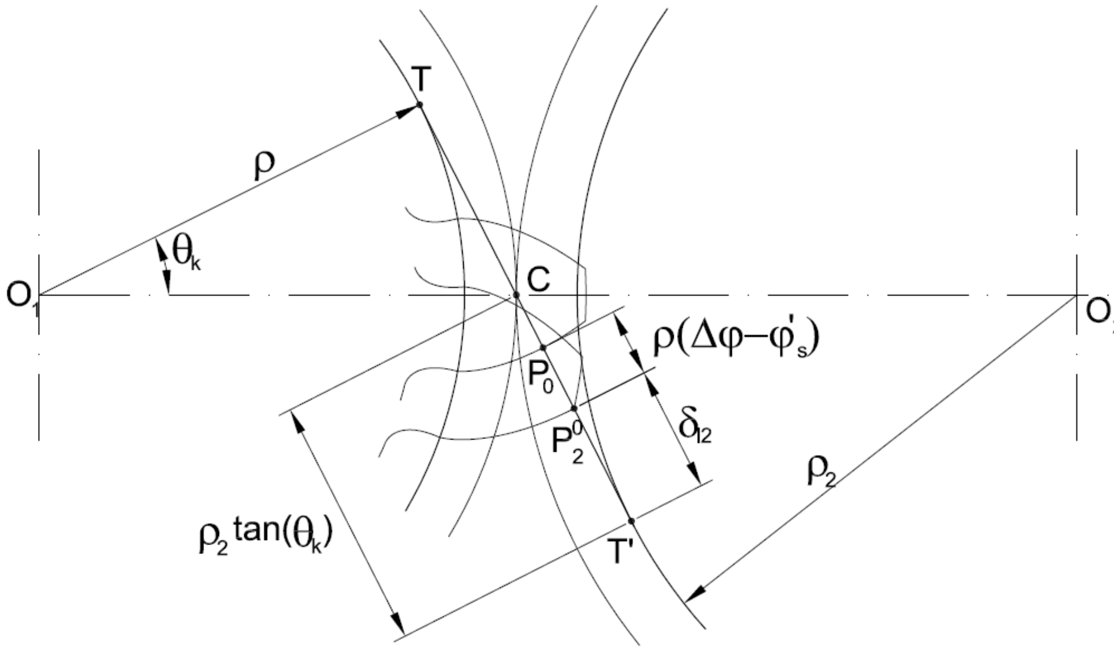

Figure 5.6 – Angular constant ϕ_s'

Now the auxiliary variable ν_a can be plotted as a function of the angular position of the driving gear and the evolution is shown in ***Figure 5.7***. In this case, however, the reset occurs at a different angular position. This phase shift between ν_m and ν_a reflects the fact that the delivery and suction control volumes are not synchronized: while one chamber is approaching the delivery region, another one is forming or expanding on the suction side. This is consistent with the operating principle of an internal gear pump with crescent separator, where suction and delivery processes occur in different angular sectors of the machine.

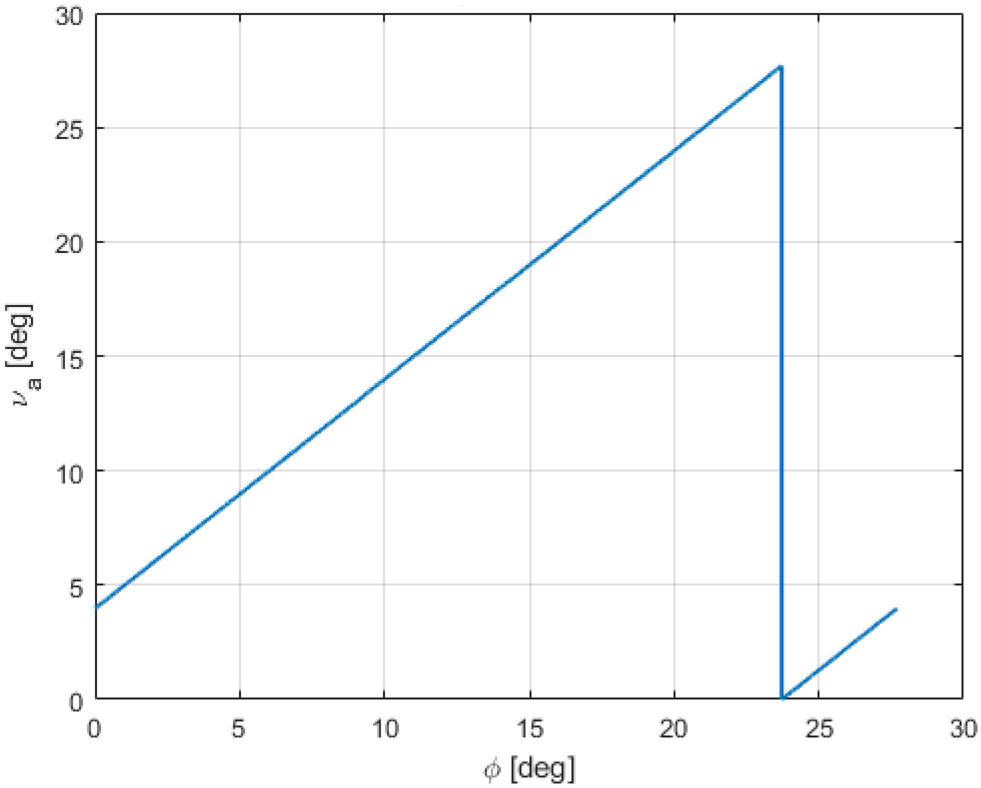

Figure 5.7 – Auxiliary suction variable plot

5.4 Radius Vectors for the Control Volumes

The core of the formulation presented in [9] lies in the use of radius vectors that define the instantaneous boundaries of the control volumes. These vectors describe the radial distance from the gear centers to the active points of the tooth profiles delimiting the fluid chambers.

Pinion Radius on the Delivery Side

The radius associated with the delivery chamber on the pinion side is:

$$R_{m1} = \sqrt{\rho^2 + (\rho\nu_m + \delta_{i1})^2} \tag{5.14}$$

This equation has a clear geometric meaning. The quantity inside the second square term is the tangent coordinate measured along the involute development starting from the active beginning of the profile. Combining this tangent coordinate with the base radius yields the instantaneous radius of the involute point bounding the chamber.

Pinion Radius on the Trapped Side

For the trapped chamber, the corresponding pinion-side radius is:

$$R_{m2}^{t} = \sqrt{\rho^2 + (\rho \nu_m + \delta_{i1} + \rho\Delta\phi)^2} \tag{5.15}$$

The additional term $\rho\Delta\phi$ accounts for the fact that the second boundary of the trapped chamber belongs to the following tooth space. Therefore, this radius is shifted by one angular pitch relative to R_{m1}.

Pinion Radius on the Suction Side

On the suction side, the pinion boundary is described by:

$$R_{m2} = \sqrt{\rho^2 + (T_T - \delta_{i2} - \rho\Delta\phi + \rho\nu_a)^2} \tag{5.16}$$

This expression reflects the opposite side of the meshing segment. The combination $T_T - \delta_{i2}$locates the useful portion of the active profile starting from the other end of the contact segment, while the shift by $-\rho\Delta\phi$ensures the correct positioning with respect to the adjacent tooth space.

Internal Gear Radius on the Delivery Side

The internal gear radius that bounds the delivery chamber is:

$$R_{c1} = \sqrt{\rho_2^2 + (\rho \nu_m + \delta_{i1} + (\rho_2 - \rho)\tan\theta_k)^2} \tag{5.17}$$

This expression is analogous to the pinion one, but an additional offset appears due to the different base circle of the internal gear. The term $(\rho_2 - \rho)\tan\theta_k$accounts for the relative translation of the involute contact coordinate between the two gears.

Internal Gear Radius on the Trapped Side

For the trapped chamber, the corresponding internal gear radius is:

$$R_{c2}^{t} = \sqrt{\rho_2^2 + (\rho \nu_m + \delta_{i1} + (\rho_2 - \rho)\tan\theta_k + \rho\Delta\phi)^2} \tag{5.18}$$

Again, the additional pitch shift identifies the second boundary of the trapped region.

Internal Gear Radius on the Suction Side

Finally, the internal gear radius on the suction side is:

$$R_{c2} = \sqrt{\rho_2^2 + (T_T - \delta_{i2} + \rho\nu_a - \rho\Delta\phi + (\rho_2 - \rho)\tan\theta_k)^2} \tag{5.19}$$

Together, these radius vectors provide the complete instantaneous geometrical description of the chamber boundaries. They are the building blocks from which the control volume derivatives are obtained.

5.5 Control Volume Derivatives

Control volumes definition

Three fluid control volumes are considered in the model:

- V_m: delivery volume,
- V_a: suction volume,
- V_t: trapped volume.

As shown in ***Figure 5.8***, the first two are the main pumping volumes, respectively connected to the delivery and suction ports. The third one is a transient sealed pocket of fluid formed between consecutive tooth contacts. Finally, V_d are constant volumes delimited by two successive teeth and the casing. In the adopted formulation, instead of deriving the closed-form expressions of the volumes themselves, it is more convenient to derive directly their derivatives with respect to the angular coordinate. This is because the instantaneous flow rate is directly related to the rate of volume change. Moreover, the geometry of each chamber can be represented as the difference between an area swept by the pinion side and an area swept by the internal gear side, multiplied by the axial width b. Since the model is two-dimensional in the transverse plane, the volumetric contribution is obtained by extrusion along the width. The factor ½ that appears in the final expressions comes from the area formula associated with polar sectors or equivalent radius-based swept regions. In essence, the chamber area variation can be written in terms of differences of squared radii; multiplying by b then converts area into volume.

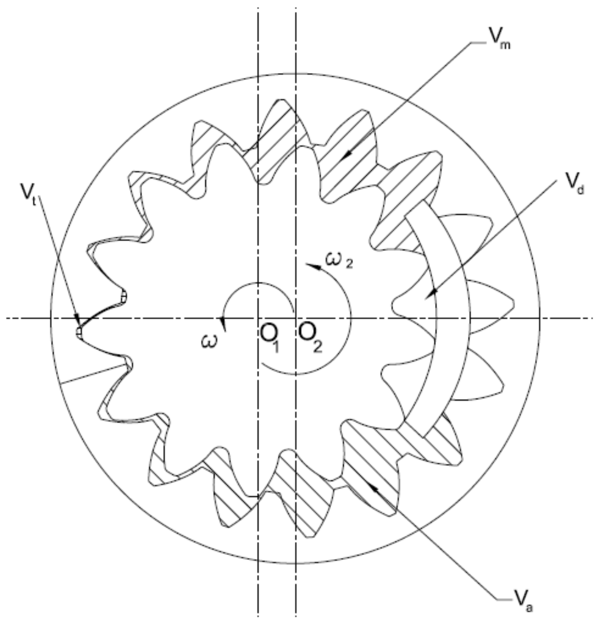

Figure 5.8 – Control volumes

Derivative of the delivery volume

The derivative of the delivery volume with respect to the pinion angular position is:

$$\frac{dV_m}{d\phi} = \frac{b}{2}\left[(R_{m1}^2 - R_e^2) - \frac{z_p}{z_r}(R_{c1}^2 - R_{f2}^2)\right] \tag{5.20}$$

This formula may be interpreted term by term. The quantity $R_{m1}^2 - R_e^2$ represents the contribution of the pinion side. It measures how the active boundary radius compares with the reference outer radius R_e. Since the chamber is delimited by the tooth profile and by the tooth tip circle, the difference between the two squared radii gives the incremental swept area. The quantity $R_{c1}^2 - R_{f2}^2$ plays an analogous role on the internal gear side, with R_{f2} acting as the reference radius. However, this contribution must be scaled by the ratio $\frac{z_p}{z_r}$. This factor arises from the kinematic relation between the angular motion of the pinion and that of the internal gear. Since the derivative is taken with respect to the pinion angle ϕ, the internal gear contribution must be converted accordingly. Physically, $\frac{dV_m}{d\phi}$ describes how fast the delivery chamber volume changes as the pinion rotates. Negative values correspond to a decreasing chamber volume, which means fluid is being expelled toward the outlet. In ***Figure 5.9***, the trend of the derivative of the delivery volume V_m is shown. The derivative $\frac{dV_m}{d\phi}$ is always negative. This confirms that the delivery chamber is continuously reducing its volume during the considered angular interval. The absolute value of the derivative represents the instantaneous geometric contribution to the delivery flow rate. The curve is not perfectly constant, but slightly varies with ϕ. This happens because the chamber boundary is not generated by a simple circular motion, but by the relative meshing of involute profiles. As the contact point moves along the tooth profiles, the effective radius vectors defining the chamber change, producing a non-uniform volume reduction. The discontinuity around $\phi \simeq 3.5°$corresponds to the reset of the auxiliary variable ν_m. This is a numerical/geometrical transition between two adjacent pitch intervals. It does not indicate an actual instantaneous physical jump of the pump flow, but the change of the active tooth-pair configuration used by the analytical model.

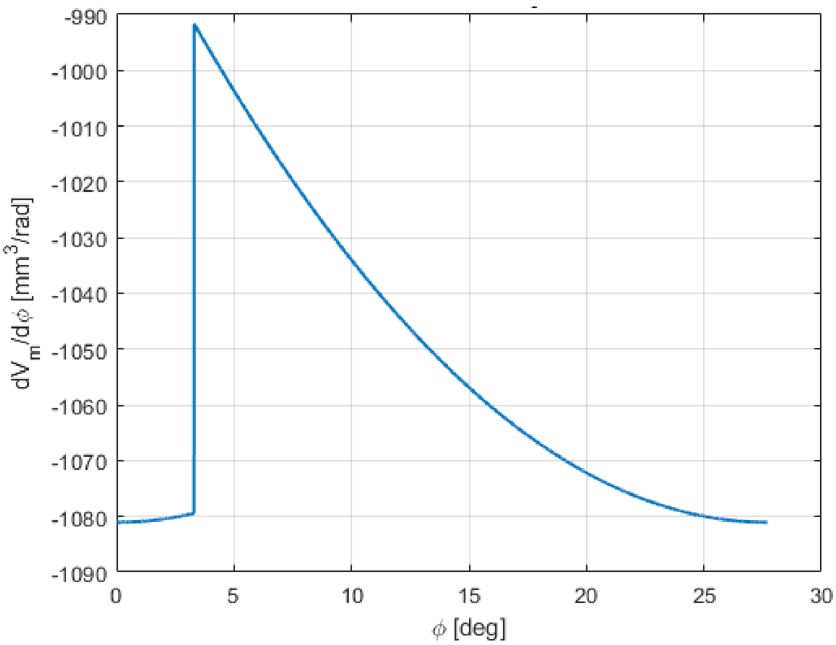

Figure 5.9 – Derivative of delivery volume

Derivative of the suction volume

The derivative of the suction volume is:

$$\frac{dV_a}{d\phi} = \frac{b}{2}\left[(R_e^2 - R_{m2}^2) - \frac{z_p}{z_r}(R_{f2}^2 - R_{c2}^2)\right] \tag{5.21}$$

This expression mirrors the previous one, but the arrangement of the terms is reversed because on the suction side the chamber grows instead of shrinking. A positive increase of the suction chamber implies that fluid is drawn into the pump from the inlet. From a continuity standpoint, this volume increase is the intake counterpart of the delivery chamber decrease. Although $\frac{dV_a}{d\phi}$ is not used directly in the final theoretical flow equation implemented in the script, it is still important because it allows reconstruction of the suction-side control volume and provides a consistency check on the chamber evolution. As shown in ***Figure 5.10***, The derivative $\frac{dV_a}{d\phi}$ is positive over the entire interval. This means that the suction chamber volume increases as the gear rotates. The positive derivative is therefore coherent with the intake process. The curve has a smooth non-linear trend, reaching a maximum and then decreasing before the reset. This is again caused by the involute meshing geometry: the rate at which the chamber opens is not constant because the contact position and the effective boundaries of the control volume evolve continuously. The vertical discontinuity near $\phi \simeq 24°$is associated with the reset of ν_a. It marks the end of one suction chamber evolution and the beginning of the next one. As for the delivery side, this discontinuity is mainly related to the modular description of the process.

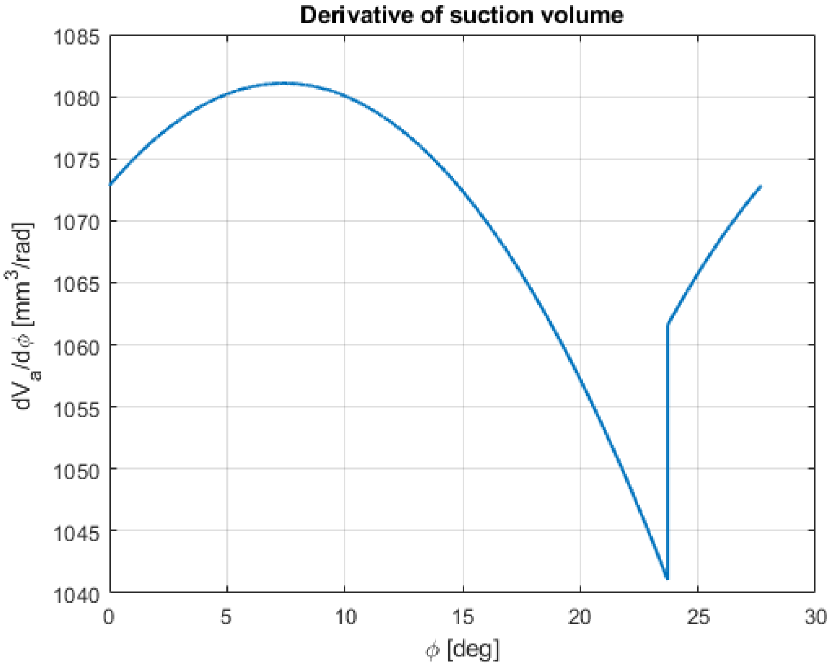

Figure 5.10 – Derivative of suction volume

Derivative of the trapped volume

The derivative of the trapped volume is first computed in raw form as:

$$\left(\frac{dV_t}{d\phi}\right)_{\text{raw}} = \frac{b}{2}\left[\left((R^t_{m2})^2 - R^2_{m1}\right) - \frac{N_d}{N_{d2}}\left((R^t_{c2})^2 - R^2_{c1}\right)\right] \tag{5.22}$$

This equation measures the evolution of the intermediate chamber enclosed between two successive tooth boundaries. However, this chamber exists only during a limited angular interval. Therefore, the physically admissible derivative is:

$$\frac{dV_t}{d\phi} = \begin{cases} \left(\frac{dV_t}{d\phi}\right)_{\text{raw}}, & \phi \in [\phi_{bt}, \phi_{et}] \\ 0, & \text{otherwise} \end{cases}$$

The trapped volume plays a major role in the shape of the instantaneous flow waveform. If the trapped volume decreases while being isolated, it may contribute to the delivery side once communication is re-established. Conversely, if it increases, it does not directly generate outlet flow. This asymmetry is the reason for the appearance of the minimum operator in the theoretical flow expression. As shown in ***Figure 5.11***, The derivative $\frac{dV_t}{d\phi}$ is zero over the portions in which the trapped volume is not active. It becomes negative after the first transition, then increases almost linearly, crosses zero, and becomes positive before returning to zero. This behaviour is typical of a trapped volume that first decreases, causing potential compression of the enclosed fluid, and then increases, causing potential decompression. In a purely geometric model, this only affects the theoretical volume balance. In a pressure-based lumped parameter model, however, this same behaviour would be responsible for trapped-oil pressure fluctuations. The fact that $\frac{dV_t}{d\phi}$ is much smaller than $\frac{dV_m}{d\phi}$ and $\frac{dV_a}{d\phi}$ confirms that the trapped volume has a secondary influence on the average displacement, but can still be relevant for local pressure peaks, noise, vibration, and flow ripple.

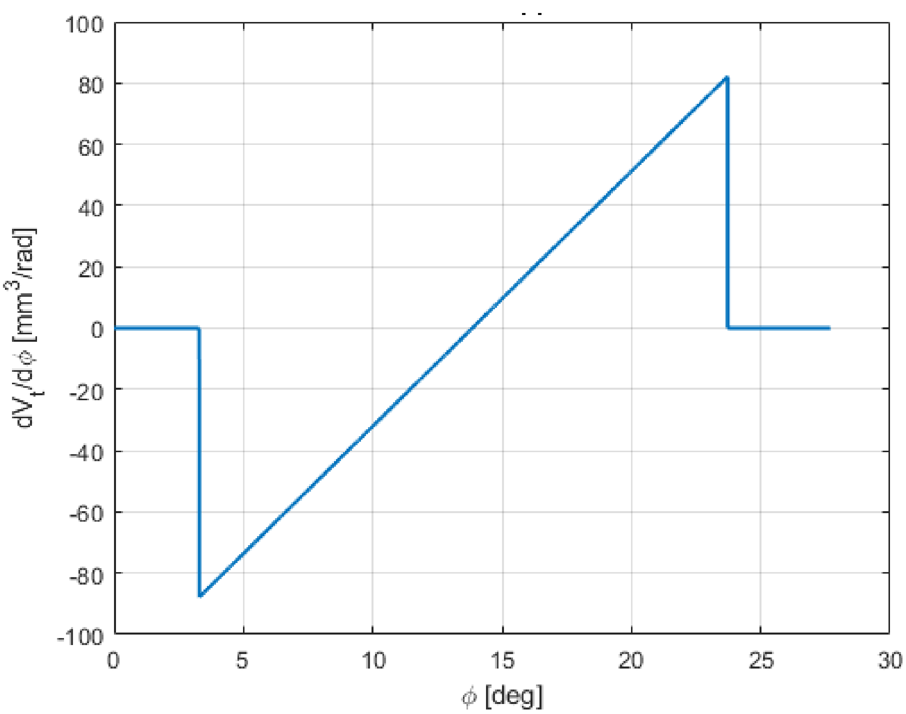

Figure 5.11 – Derivative of trapped volume

Reconstruction of the Volumes

Although the theoretical flow equation only requires the derivatives of the control volumes, the actual volumes can be reconstructed by integration. For the delivery and suction chambers:

$$V_m(\phi) = \int \frac{dV_m}{d\phi}\, d\phi \tag{5.23}$$

$$V_a(\phi) = \int \frac{dV_a}{d\phi}\, d\phi \tag{5.24}$$

In the MATLAB implementation, these are evaluated numerically using cumulative trapezoidal integration:

$$V_m = \text{cumtrapz}(\phi, \frac{dV_m}{d\phi}) \tag{5.25}$$

$$V_a = \text{cumtrapz}(\phi, \frac{dV_a}{d\phi}) \tag{5.26}$$

For the trapped volume, the same approach is applied only over the interval where the chamber exists:

$$V_t = \int \frac{dV_t}{d\phi}\, d\phi \tag{5.27}$$

with a subsequent normalization so that the minimum value is set to zero. This reconstruction has mainly a visualization purpose. It makes it possible to plot the evolution of the three control volumes and to verify whether their behaviour is physically consistent with the operating principle of the pump.

5.6 Flow Rate and Flow Ripple Calculation

Instantaneous Flow Rate

The instantaneous theoretical flow rate is written as:

$$Q_{th}(\phi) = -\omega\left(\frac{dV_m}{d\phi} + \min\left(\frac{dV_t}{d\phi}, 0\right)\right) \tag{5.28}$$

This equation encapsulates the physical meaning of the geometric model. The factor ω converts the derivative with respect to angular position into a time derivative, since:

$$\frac{dV}{dt} = \frac{dV}{d\phi}\frac{d\phi}{dt} = \omega\frac{dV}{d\phi} \tag{5.29}$$

The minus sign is necessary because delivery is associated with a decrease of the delivery chamber volume. If V_m decreases, then $\frac{dV_m}{d\phi} < 0$, and the flow delivered to the outlet must be positive. The term involving the trapped volume requires special care. Only the negative part of $\frac{dV_t}{d\phi}$ is included through:

$$\min\left(\frac{dV_t}{d\phi}, 0\right)$$

This means that only when the trapped volume decreases does it contribute to the delivered flow. If the trapped volume is increasing, it is merely storing fluid within the sealed chamber and does not yet supply the outlet. This point is important both mathematically and physically.

The trapped chamber is not permanently connected to the delivery port. Therefore, its influence on the outlet flow depends on whether it is releasing or accumulating fluid. The theoretical flow-rate (***Figure 5.12***) plot shows a periodic fluctuation around an average value close to 9.8 L/min. The minimum occurs approximately at the middle of the angular pitch. This ripple is generated by the non-uniform variation of the control volumes. Even in an ideal geometric model, the instantaneous displaced volume is not perfectly constant because the meshing process is governed by involute profiles and by the cyclic transition between tooth chambers. The curve is smooth except for the effects associated with the pitch transition. The amplitude of the fluctuation is relatively small, which indicates that the pump geometry provides a reasonably continuous delivery. However, this residual ripple is important because, in real operation, it may contribute to pressure pulsations and acoustic excitation.

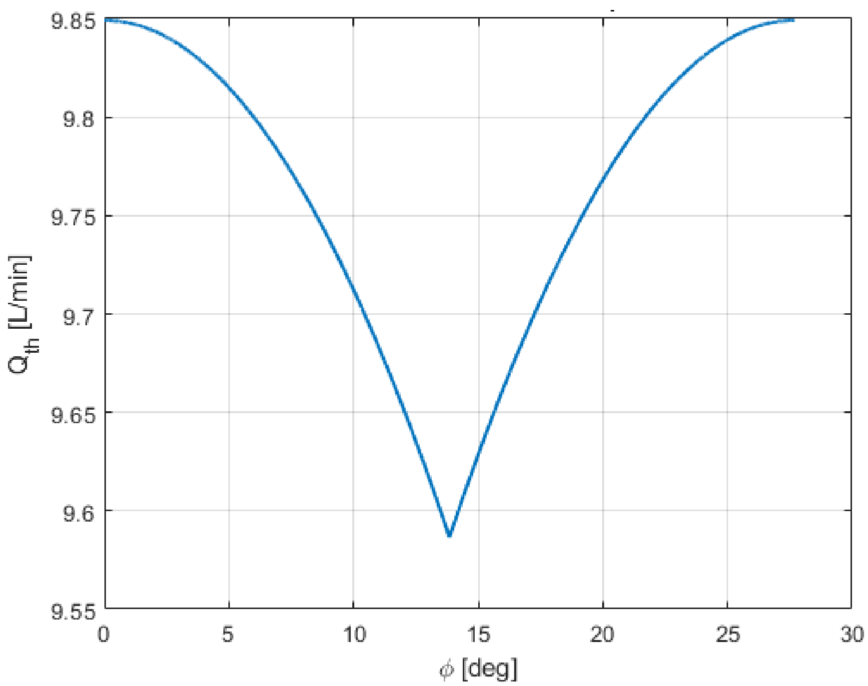

Figure 5.12 – Theoretical flow at 1450 rpm

Mean Flow Rate

Once $Q_{th}(\phi)$ has been obtained over one angular pitch, the mean theoretical flow rate can be computed as:

$$Q_{\text{mean}} = \frac{1}{\Delta\phi} \int_0^{\Delta\phi} Q_{th}\,(\phi)\, d\phi \qquad (5.30)$$

In the numerical implementation, this quantity is approximated by the arithmetic mean of the discrete values of Q_{th}, which is equivalent to the integral average under uniform angular discretization.

Flow Ripple Definition

Because the chamber volumes do not vary uniformly during rotation, the instantaneous flow rate is not constant. Instead, it oscillates around its mean value. This phenomenon is known as flow ripple. The maximum and minimum instantaneous flow rates are:

$$Q_{\max} = \max(Q_{th}(\phi)) \tag{5.31}$$
$$Q_{\min} = \min(Q_{th}(\phi)) \tag{5.32}$$

The ripple amplitude is then:

$$\Delta Q = Q_{\max} - Q_{\min} \tag{5.33}$$

and the relative ripple, expressed as percentage of the mean flow rate, is:

$$\delta_Q = 100 \frac{\Delta Q}{Q_{\text{mean}}} \tag{5.34}$$

The obtained results are shown in **Table 5.1**.

Parameter	Value	Units
Q_{mean}	9.76	[l/min]
$Q_{\max}$	9.85	[l/min]
$Q_{\min}$	9.58	[l/min]
ΔQ	0.26	[l/min]
δ_Q	3.84	%

Table 5.1 - Flow rate results

5.7 Pump Displacement

The theoretical displacement per revolution is related to the mean flow rate and the rotational speed. If the speed is expressed in revolutions per minute, the displacement in cm^3/rev can be written as:

$$V_g = \frac{Q_{\text{mean},L/min} \cdot 1000}{n_{\text{rpm}}} \tag{5.35}$$

Where the multiplication by 1000 converts liters into cubic centimeters. Theoretical displacement is one of the most important quantities for validating the reconstructed geometry.

6 Functional Analysis

6.1 Beginning of the Meshing Cycle

Also for this functional analysis, as said in Chapter 5, It's convenient to identify three fluid control volumes as shown in ***Figure 6.1***:

- V_m: delivery volume,
- V_a: suction volume,
- V_t: trapped volume.

V_d are the transport volumes along the crescent and are constant volumes delimited by two successive teeth and the housing. At the beginning of the meshing cycle, a new inter-teeth chamber is progressively generated between adjacent tooth profiles of the pinion and the internal gear. As the gears rotate, a new contact point is established between the mating teeth, gradually isolating the different fluid volumes from the neighbouring chambers as shown in ***Figure 6.1***. At this stage, the crescent separator divides the pump into two distinct hydraulic regions:

- the suction side,
- and the delivery side.

From a kinematic perspective, the beginning of a new meshing interval is identified through the local meshing variable:

$$\nu_m = 0$$

where ν_m represents the local angular coordinate associated with the tooth pitch interval and is periodically reset at each new meshing cycle as reported in Chapter 5.
By analysing the plot of ν_m, the pinion angular position associated with the reset condition of the local meshing cycle can be determined and, in fact, the CAD reconstruction shows that this condition occurs at an angular position of the pinion close to about $-4°$.
However, the condition $\nu_m = 0$ does not necessarily correspond to:

- a zero absolute angular position of the pinion,
- the minimum chamber volume condition,
- nor the exact onset of the effective suction phase.

The variable ν_m identifies the beginning of a new kinematic meshing interval, namely the formation of a new contact point between the conjugate tooth profiles. Nevertheless, the real hydraulic behaviour of the pump is additionally influenced by the compensation plate geometry and by trapped oil discharge phenomena.
The CAD analysis shows that, immediately after the formation of the new meshing point, the confined chamber may continue decreasing slightly before the actual volumetric expansion begins. This behaviour is physically consistent with the presence of a relief groove machined on the compensation plate as shown in ***Figure 6.2***.
In fact, during the initial phase of the meshing cycle, the newly confined chamber is still temporarily connected to the delivery side through the unloading groove. As a consequence,

the trapped fluid remains at delivery pressure even after the chamber has been kinematically isolated by the new tooth contact. During this short transition interval:

- the chamber is already geometrically confined,
- it is not yet operating as an effective suction volume.

The unloading groove allows the discharge of the trapped high-pressure fluid, reducing trapped oil compression effects and preventing excessive pressure peaks. Only after this hydraulic communication is interrupted does the chamber start its effective volumetric expansion, generating the low-pressure condition responsible for the suction process.
Therefore, the beginning of the meshing interval identified in the [9] formulation should be interpreted as the onset of a new kinematic cycle rather than the exact beginning of the suction phase from a fluid-dynamic standpoint.

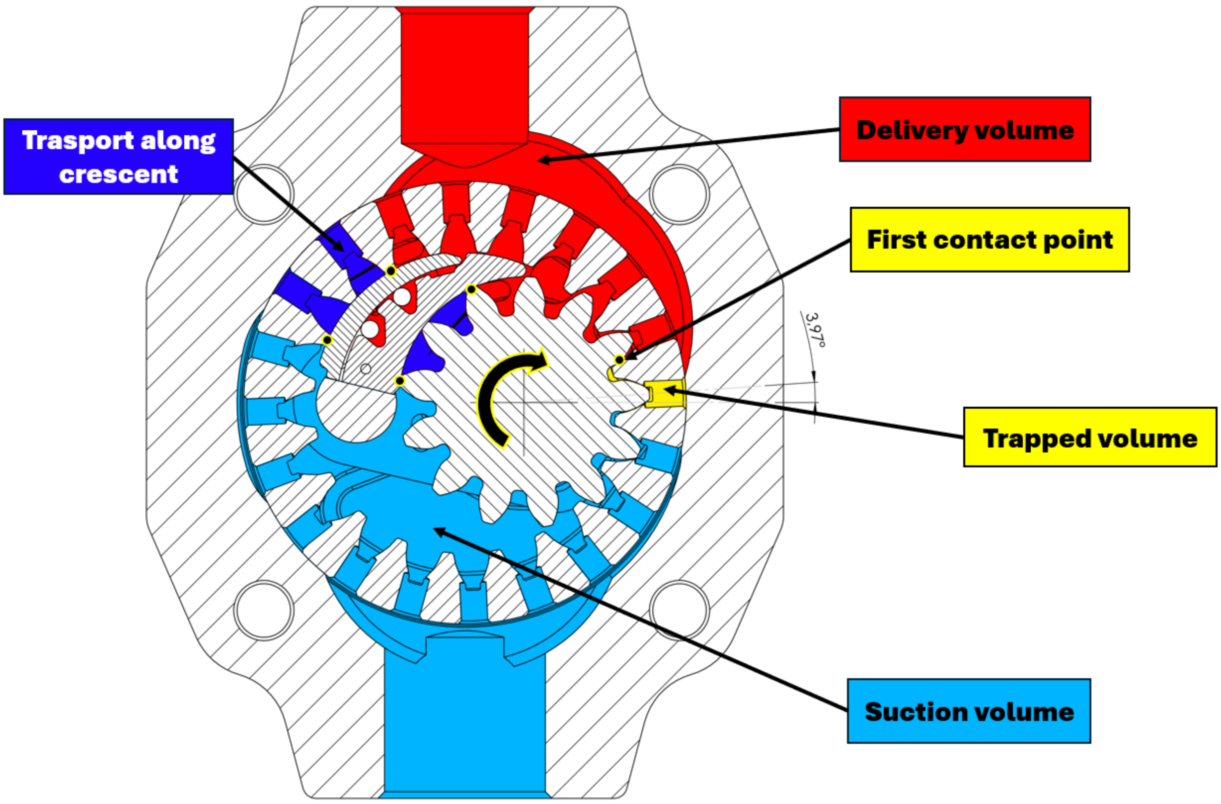

Figure 6.1 – Volumes formation at beginning of meshing cycle

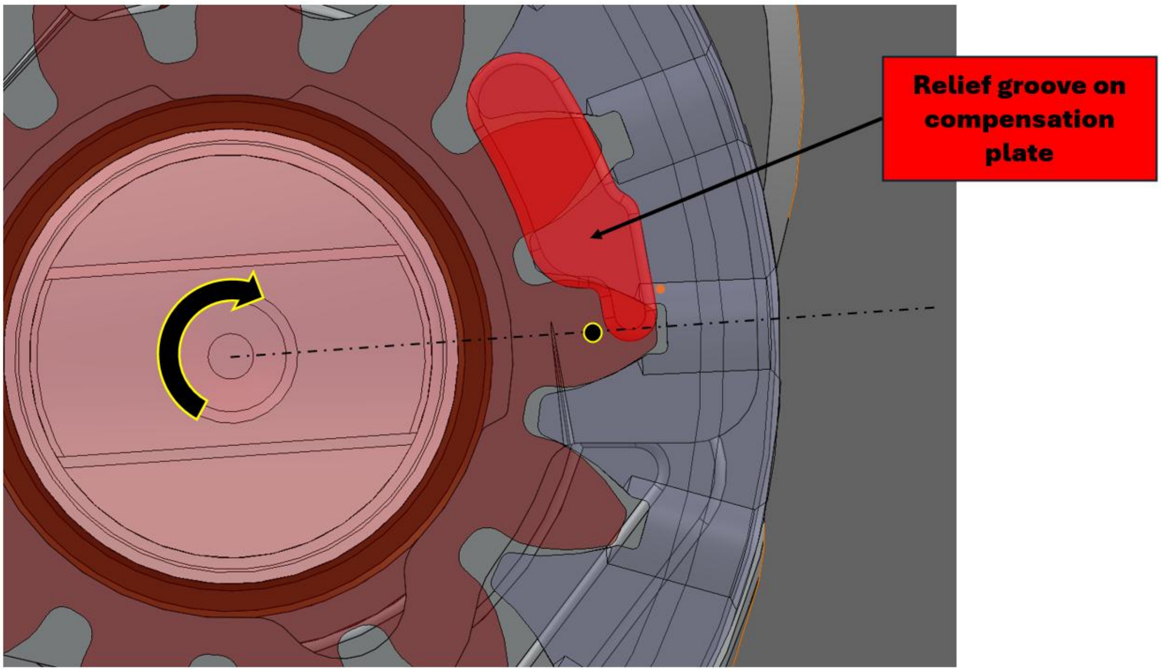

Figure 6.2 – Relief groove on suction side

6.2 Expansion Phase and Suction Process

As the rotation of the driving gear continues, at an angular position close to about 0° the pression of trapped volume, pass gradually from the delivery pression value to the suction pression value thanks to a triangular groove machined on the compensation plate as shown in ***Figure 6.3***. So, the role of this triangular groove is to mitigate the pressure peaks generated by trapped oil phenomena because the trapped chamber volume may either decrease or increase depending on the instantaneous meshing configuration. This phenomenon can produce:

- localized pressure peaks,
- cavitation conditions,
- pressure ripple,
- noise generation,
- and additional mechanical loads on the gears and bearings.

The trapped volume phenomenon is particularly important in real operating conditions because the fluid is not perfectly incompressible. Consequently, even small variations in chamber volume can generate significant pressure fluctuations.
Although trapped oil dynamics are not directly included in the purely geometric formulation of the theoretical flow rate, they become essential when extending the model toward:

- lumped parameter approaches,
- pressure analysis,
- or CFD simulations.

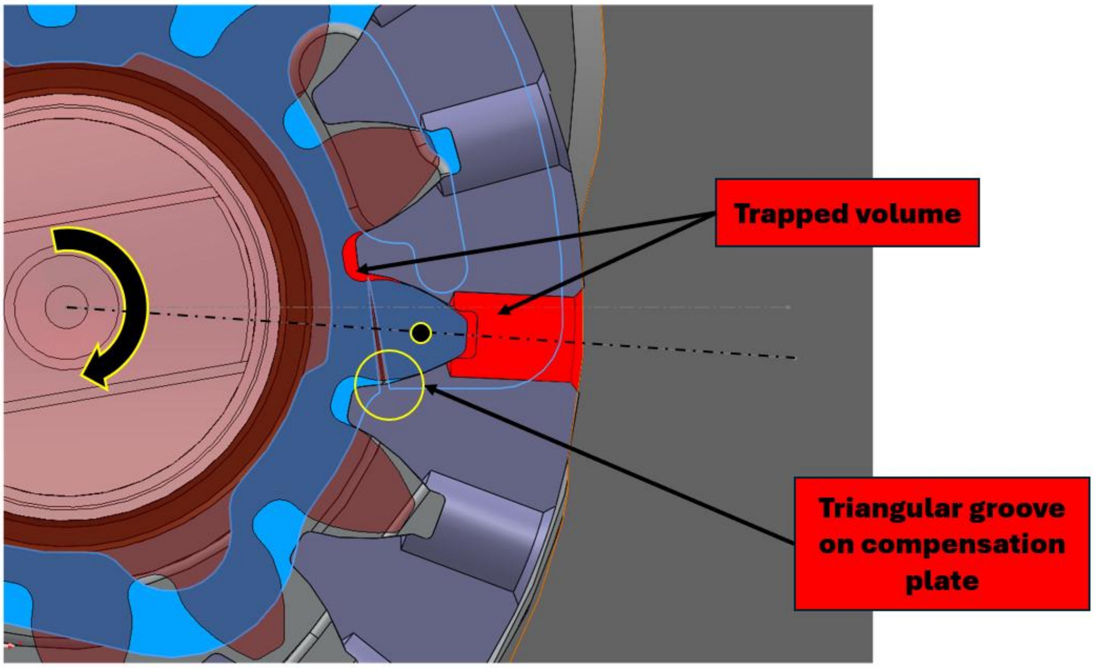

Figure 6.3 – Role of the triangular groove on suction side

Then the mating teeth progressively separate and this relative motion generates an increase in the inter-teeth chamber volume. The volumetric expansion produces a local pressure decrease inside the chamber, promoting the suction of fluid from the inlet port. Therefore, the pumping action is not generated by a direct pushing mechanism, but rather by the continuous variation of the enclosed control volumes produced by the meshing kinematics. During this phase, the suction volume continuously increases until reaching its maximum value approximately when a new contact point is generated.

6.3 Transport of the Fluid Along the Crescent

The crescent separator prevents direct communication between the suction and delivery regions, forcing the fluid to follow the peripheral path along the housing. After the suction phase, the fluid remains confined inside the inter-teeth chamber and is transported along the crescent separator toward the delivery region. In this phase, the chamber volume remains approximately constant compared to the rapid variations occurring during the expansion and compression stages. The primary function of the crescent separator is to maintain hydraulic separation between the low-pressure and high-pressure regions of the pump. The geometry and positioning of the crescent are particularly important because they influence:

- the sealing effectiveness,
- leakage paths,
- local pressure gradients,
- and trapped oil phenomena.

The crescent also guides the fluid along the peripheral trajectory imposed by the relative rotation of the gears. This mechanism allows the transported volume to progressively move from the suction side toward the delivery side without direct recirculation. ***Figure 6.4*** shows the transport phase of the fluid along the crescent separator.

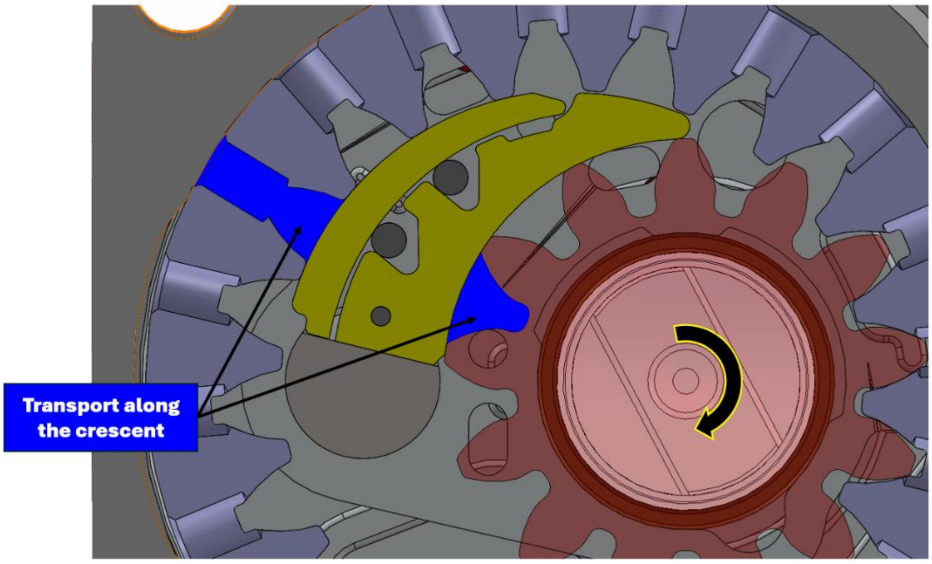

Figure 6.4 – Transport of the fluid along the crescent

6.4 Compression Phase and Delivery Process

The role of the groove on the housing shown in ***Figure 6.5*** is to distribute the delivery pressure in specific zones and, in particular, to ensure the crescent elements and compensation plates movements. As shown in ***Figure 6.6***, two distinct categories of passages can be identified within the compensation plate: pressurization holes, located in the upper region and intended to distribute delivery pressure for hydraulic compensation purposes, and lubrication holes, located near the shaft support area and primarily intended to supply oil to the bushings and adjacent sliding interfaces. As shown in ***Figure 6.7***, the delivery pressure acting on the inner surfaces of the crescent elements ensure the contact between the inner and outer crescent and the gearset ensuring, in this way, the radial gap compensation. In particular, the delivery pressure in the housing groove mentioned before, acting on the compensation plate surface, generate an axial force that ensure the axial gap compensation. As shown in ***Figure 6.7***, the delivery pressure acts on dedicated compensation areas, generating a force that presses the crescent segments against the gearset and enables radial compensation. The sizing and the ratio of these pressure-loaded surfaces, together with the sealing rolls located between the segment and the segment carrier, is carefully engineered to achieve a resultant force that move the crescent elements toward the gears in order to have a nearly gap-free contact, thus reducing internal leakage and improving sealing effectiveness. Moreover, as shown in ***Figure 6.8***, spring elements positioned beneath the sealing rolls provide the preload required to maintain effective contact even under low-pressure operating conditions. Moreover, as shown in ***Figure 6.9***, the delivery pressure acting on the inner surfaces of the compensation plates ensure the contact between the compensation plates and the gearset ensuring, in this way, the axial gap compensation. Also in this case, the sizing and the ratio of the pressure-loaded surfaces is carefully engineered to achieve a resultant force that move the compensation plates toward the gearset in order to have a nearly gap-free contact, thus reducing internal leakage and improving sealing effectiveness. As said before, small holes are present in the compensation plate in correspondence with the shaft support region. Based on their position and geometry, these features are believed to primarily serve a lubrication function. No direct evidence was found indicating that these passages are involved to pressure balancing or volumetric sealing.

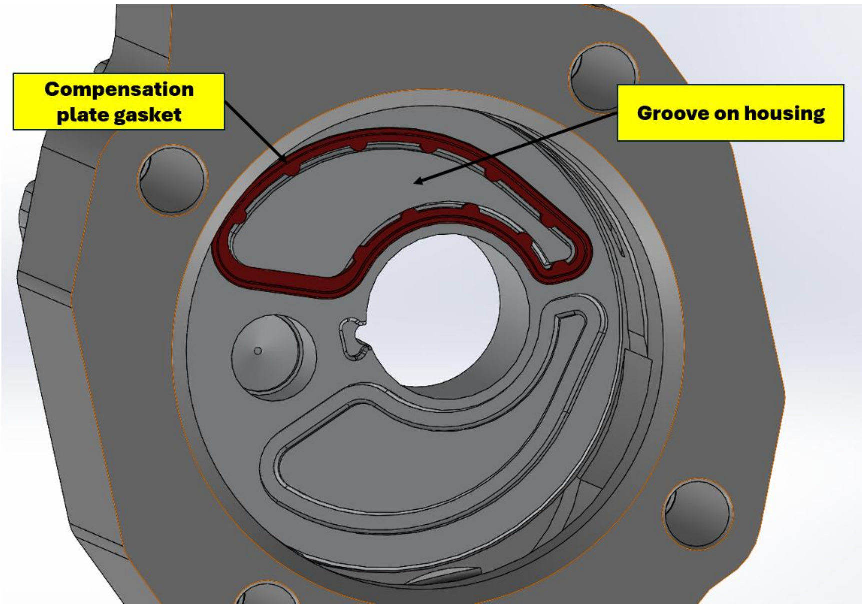

Figure 6.5 – Housing features

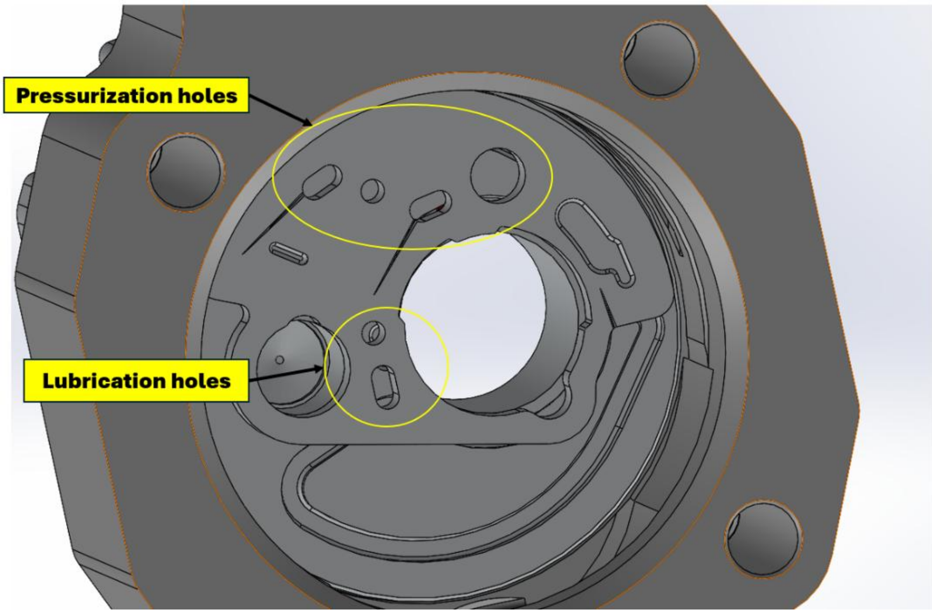

Figure 6.6 – Holes on compensation plate

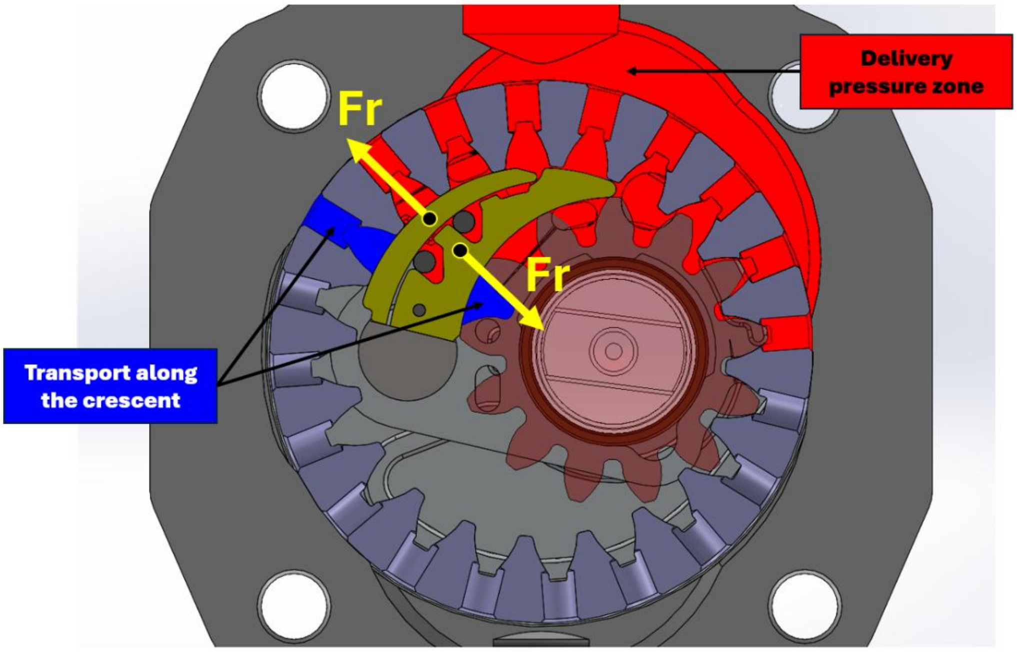

Figure 6.7 - Delivery pressure region and radial compensation

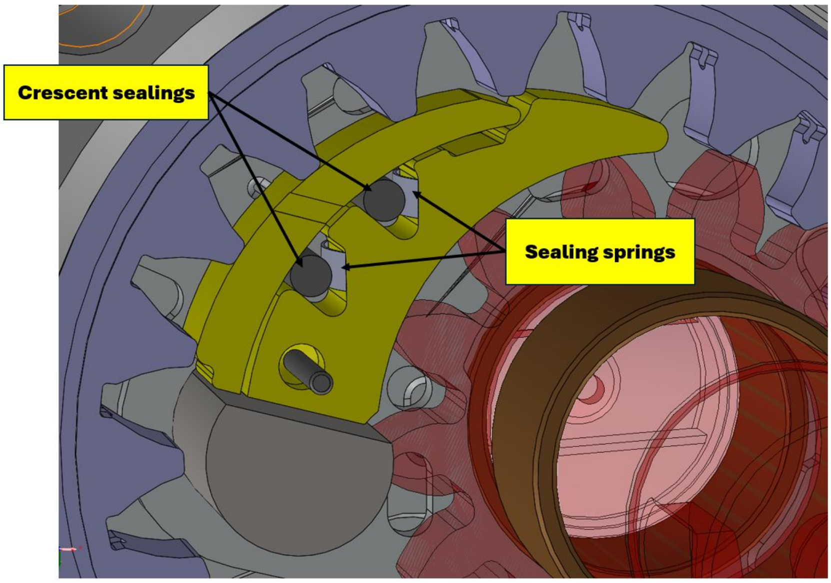

Figure 6.8 – Sealing rolls and sealing springs

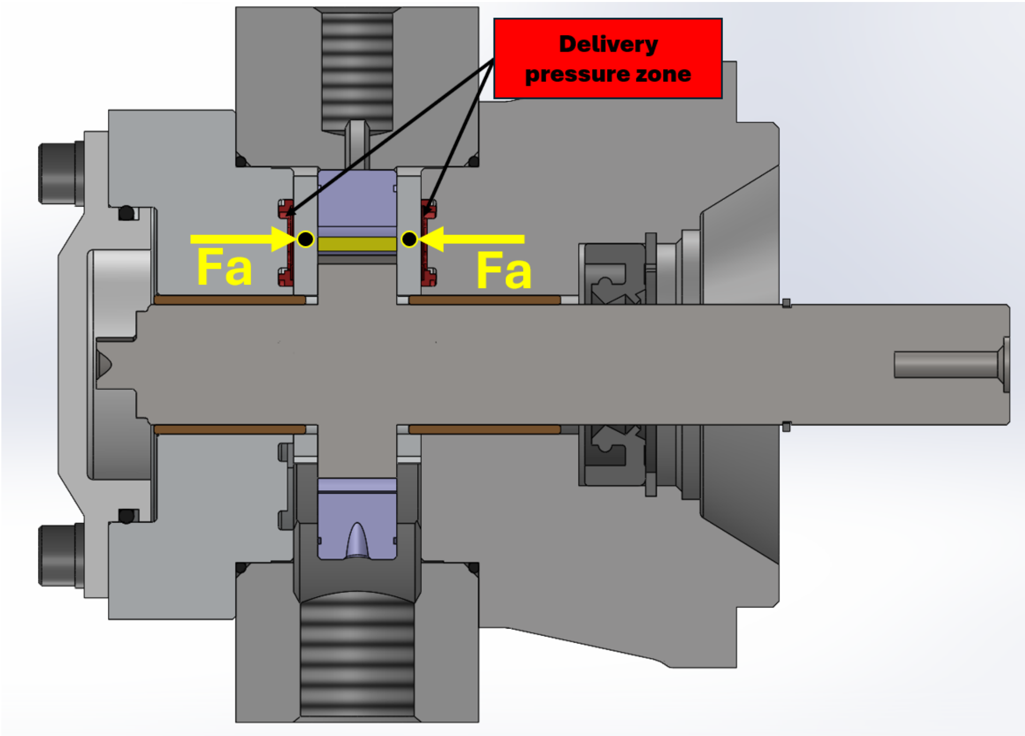

Figure 6.9 – Delivery pressure region and axial compensation

A dedicated pressure passage can be observed in one of the compensation plates as shown in ***Figure 6.10***, connecting the delivery region to the housing of the sealing roll. Its geometry suggests that it may serve to hydraulically pressurize the sealing roll seat. During the transport phase of the fluid along the crescent separator the fluid is trapped between adjacent tooth profiles and is carried circumferentially around the pump without experiencing significant volume variations. Consequently, the chamber pressure remains approximately constant and close to the suction pressure level. As the gears continue to rotate, the transport chamber approaches the delivery region. A direct connection between a low-pressure chamber and the delivery port would generate a sudden pressure rise, resulting in pressure shocks, and additional noise emissions. As shown in ***Figure 6.11***, in order to mitigate these effects, also in this case the compensation plate is provided with specially designed triangular grooves located upstream of the delivery port. When the transport chamber reaches this region, a gradual hydraulic communication is established with the delivery side through the triangular grooves. Owing to their progressively increasing cross-sectional area, the grooves allow a controlled amount of high-pressure fluid to enter the chamber. As a result, the chamber pressure increases smoothly from the transport pressure level toward the delivery pressure. The pressurization process therefore occurs progressively rather than instantaneously and this gradual pressure equalization reduces pressure transients.

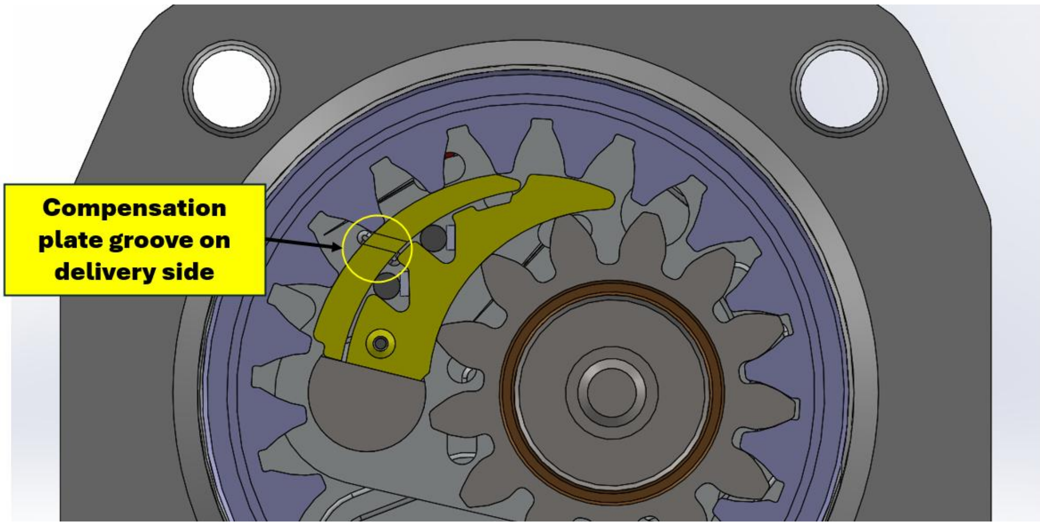

Figure 6.10 – Compensation plate pressurization groove on delivery side

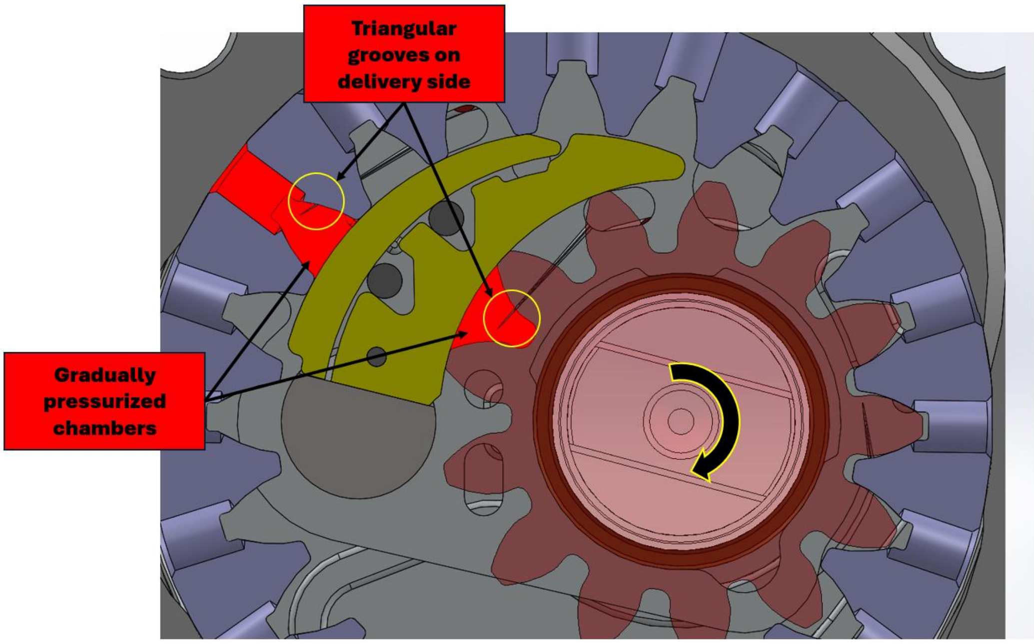

Figure 6.11 – Compensation plate triangular grooves on delivery side

As the chamber approaches the delivery region, the meshing teeth progressively reduce the delivery volume. The decreasing chamber volume produces a pressure increase inside the trapped fluid region. Once communication with the delivery port is established, the pressurized fluid is expelled from the chamber toward the outlet section of the pump. The delivery process is therefore generated by the progressive re-engagement of the tooth profiles, which forces the fluid out of the shrinking inter-teeth volume.

7 Results

7.1 Discussion and Comparison with Manufacturer Data

The present work focused on the reverse engineering and theoretical analysis of a crescent-type internal gear pump, with the objective of reconstructing its main geometric characteristics and evaluating its theoretical hydraulic performance through an analytical approach coherent with the formulations proposed in the scientific literature for crescent pumps. The entire activity was developed starting from the physical disassembly of the pump and from the subsequent acquisition of its geometric parameters. The reverse engineering procedure included direct measurements performed using calipers and dimensional inspection techniques, together with CAD reconstruction of the main components. The developed CAD model allowed the reconstruction of the kinematic relationships between the driving gear, the driven internal gear, and the crescent partition. Such reconstruction represented the basis for the implementation of the mathematical model in MATLAB, where the theoretical evolution of the inter-tooth chamber volumes was evaluated as a function of the angular position of the gears. The implemented model follows a purely geometric approach, consistent with the analytical formulations proposed in [9] for crescent pumps. The obtained results demonstrated the strong influence of the gear geometry on the hydraulic characteristics of the pump. In particular, the number of teeth, the involute profile development, and the geometric interaction between the gears and the crescent partition directly affect the volumetric evolution of the chambers and consequently the flow ripple behaviour. The reconstructed model provided a theoretical displacement very close to the nominal value declared by the manufacturer. This result represents one of the most important validations of the entire reverse engineering procedure, since the displacement of a positive displacement machine is directly related to the correctness of the reconstructed geometry. A comparison between the theoretical results obtained from the developed model and the reference values reported in the Rexroth technical documentation is presented in ***Table 7.1***.

Parameter	Theoretical Model	Manufacturer Data	Deviation
Displacement [cm³/rev]	6.73	6.5	+3.57%
Theoretical flow rate [L/min]	9.76	9.4	+3.84%

Table 7.1 – Data comparison

The comparison shows a good agreement between the reconstructed model and the manufacturer specifications. In particular, the deviation observed for the displacement remains below 4%, indicating that the adopted reverse engineering methodology was able to reproduce the main geometric characteristics of the original pump with satisfactory accuracy. It should be noted that the flow rate reported by the manufacturer does not represent a purely theoretical quantity. According to the technical documentation, the nominal flow rate is measured under standardized operating conditions, typically at a pressure differential of approximately 10 bar. Consequently, the manufacturer value already includes the effects of volumetric losses that occur during real pump operation. For this reason, the flow rate predicted by the present model is expected to be slightly higher than the value reported in the datasheet. Nevertheless, despite the good agreement obtained, it is important to underline that the implemented model is based on several simplifying assumptions. The developed formulation is fundamentally a geometric theoretical model and therefore does not fully account for dissipative hydraulic phenomena and mechanical effects that occur during the real operation of the pump. In particular, the theoretical formulation assumes:

- incompressible fluid behaviour;
- constant rotational speed;
- absence of pressure fluctuations;
- perfectly rigid bodies;
- absence of elastic deformations;
- ideal sealing conditions.

Under real operating conditions, several additional effects influence the effective flow rate and volumetric efficiency of the pump. One of the main sources of discrepancy between theoretical and real behaviour is represented by leakage phenomena. In crescent pumps, volumetric losses mainly originate from:

- axial leakage between the gear lateral surfaces and the compensation plates;
- radial leakage between the gear tips and the crescent partition;
- internal recirculation through clearance gaps;
- local pressure-driven backflow mechanisms.

Such effects become increasingly important at higher operating pressures, where pressure gradients across the clearances generate additional leakage flows that reduce the effective delivered flow rate. Moreover, the real pump operation is influenced by elastic and dynamic phenomena that are neglected in the present model. Gear micro-motion, shaft eccentricities, bearing compliance, and local deformations induced by pressure loads may modify the effective chamber volumes during operation. These aspects may alter the instantaneous flow evolution and contribute to additional flow ripple components. Another possible source of uncertainty is associated with the reverse engineering measurements themselves. Although the CAD reconstruction was performed with considerable attention, small dimensional errors may arise from:

- measurement tolerances;
- limited accessibility of some geometrical regions;
- scanning approximations;
- reconstruction of the involute profile;
- estimation of pressure angles and root radii.

However, the reduced deviation obtained with respect to the manufacturer data suggests that such uncertainties remained sufficiently limited and did not significantly affect the overall validity of the model. Overall, the results confirm the effectiveness of the adopted reverse engineering methodology and demonstrate that the analytical formulation derived from the literature provides a reliable prediction of the ideal hydraulic behaviour of the investigated crescent pump. The close agreement obtained for the displacement, together with the small and physically justified difference observed in the flow rate, supports the validity of the reconstructed geometry and of the implemented mathematical model.

8 Conclusions

The work presented in this thesis demonstrated the feasibility and effectiveness of a reverse engineering methodology applied to a crescent-type internal gear pump. Starting from the physical component analysis and from the reconstruction of the gear geometry, it was possible to develop a coherent analytical model capable of reproducing the main theoretical operating characteristics of the pump. The combination of CAD reconstruction, parameter identification, and MATLAB implementation allowed the complete definition of the geometric pumping mechanism and the evaluation of the theoretical displacement and flow rate characteristics. One of the main achievements of the work consists in the good agreement obtained between the developed model and the manufacturer reference data. Such correspondence confirms both the validity of the reverse engineering activity and the consistency of the analytical formulations adopted for the volumetric analysis. The developed methodology may also be extended to similar positive displacement machines, providing a useful engineering tool for performance estimation, preliminary design activities, and functional analysis of hydraulic pumps whose original design data are unavailable. Despite the satisfactory results obtained, several aspects may be further investigated in future developments. A first possible extension concerns the implementation of a more advanced leakage model capable of evaluating pressure-dependent volumetric losses through the radial and axial clearances. Such approach would allow a more realistic estimation of the effective volumetric efficiency under different operating conditions. Another important development could involve the introduction of pressure dynamics and fluid compressibility effects through lumped parameter models or dedicated hydraulic simulation environments such as AMESim or Simcenter. These approaches would allow the simulation of transient pressure distributions and dynamic flow ripple phenomena. Additional improvements may also include:

- CFD simulations of the internal flow field;
- thermo-viscous fluid analysis;
- elastohydrodynamic interaction models;
- dynamic gear micro-motion analysis;
- structural deformation evaluation under pressure loads.

Experimental validation activities could also significantly improve the reliability of the developed model. Direct measurements of delivered flow rate, pressure ripple, noise emission, and volumetric efficiency would provide additional validation of the theoretical predictions and would allow a more accurate calibration of the leakage parameters.

Appendix A: MATLAB Code

```
clear; clc; close all;
% 1) INPUT DATA FROM CAD / REVERSE ENGINEERING

% ---- Gears data ----
Nd      = 13;              % pinion teeth number
Nd2     = 20;              % internal gear teeth number
m0      = 2.5e-3;          % module [m]
theta0  = deg2rad(25);     % cutting pressure angle [rad]
Ik      = 8.8e-3;          % working center distance [m]
b       = 13e-3;           % axial width [m]

% ---- Pinion geometry ----
Re      = 18.75e-3;        % tip radius of pinion [m]
Ri      = 14.75e-3;        % start involute radius of pinion [m]
Rt      = 18.55e-3;        % end involute radius of pinion [m]


% ---- Internal gear geometry ----
Rf2     = 22.5e-3;         % root radius of internal gear [m]
Rfe2    = 22.92e-3;        % end involute radius of internal gear [m]

% ---- Crescent angles ----
% kept here for completeness, but NOT used in pure theoretical flow
chiAS   = deg2rad(20);
chiAE   = deg2rad(20);
chiMS   = deg2rad(20);
chiME   = deg2rad(20);

% ---- Phase shift between gears ----
DeltaPhi_c = 0;            % set from CAD if known

% 2) OPERATING SPEED
n_rpm   = 1450;
omega   = 2*pi*n_rpm/60;   % rad/s

% 3) MANUFACTURER REFERENCE
Vg_decl_cm3_rev = 6.5;
Q_decl_L_min    = 9.4;

% 4) BASIC GEOMETRY
% Brussani Chapter 1 (2.1 pag 9)
Rp0     = Nd  * m0 / 2              % cutting pitch radius
Rp02    = Nd2 * m0 / 2
```

```
thetak  = acos(((Rp02 - Rp0)/Ik) * cos(theta0)) % working pressure angle
thetakdeg  = rad2deg(acos(((Rp02 - Rp0)/Ik) * cos(theta0))) % working pressure angle

Rpl    = Rp0  * cos(theta0) / cos(thetak)      % working pitch radius pinion
Rpl2    = Rp02 * cos(theta0) / cos(thetak)      % working pitch radius internal gear

rho     = Rp0  * cos(theta0)                 % base radius pinion
rho2    = Rp02 * cos(theta0)                 % base radius internal gear

DeltaPhi  = 2*pi/Nd                       % angular pitch pinion
DeltaPhi2 = 2*pi/Nd2                      % angular pitch internal gear


% 5) UNUSED PARTS OF CONTACT SEGMENT
% Brussani Chapter 1 - internal gears (2.1 pag 11)
TT = (rho + rho2) * tan(thetak)

delta_i2 = TT - sqrt(max(Rt^2 - rho^2, 0))

term1 = sqrt(max(Rfe2^2 - rho2^2, 0)) - (rho2 - rho) * tan(thetak)
term2 = sqrt(max(Ri^2   - rho^2,  0))
delta_i1 = max(term1, term2)

% 6) AUXILIARY ANGULAR VARIABLES
% Brussani Chapter 4 (pag 56)
nu0   = delta_i1 / rho %2.3
gamma = acos(rho / Rpl) %

% evolvente(theta) = tan(theta) - theta
phi1_p = evolvente(thetak) - evolvente(gamma) %2.4

phi_s  = tan(thetak) - nu0 + phi1_p %2.2

nu20   = delta_i2 / rho2 %2.9
phi_s_p = DeltaPhi - phi1_p + (Nd2/Nd) * tan(thetak) + nu20 %2.8

% trapped volume creation / disappearance angles
phi_bt = DeltaPhi - phi_s %3.18
phi_et = DeltaPhi - phi_s_p %3.19

% 7) ANGULAR GRID -----DISCRETIZZAZIONE
N_pts = 6000;
phi = linspace(0, DeltaPhi, N_pts);

% Auxiliary variables
nu_m = mod(phi + phi_s,   DeltaPhi) %mandata
nu_a = mod(phi + phi_s_p, DeltaPhi) %aspirazione
```

```
% 8) RADIUS VECTORS - CASE "POMPE CON LUNETTA" pag 72
% Brussani Chapter 4, Eqs. 4.86-4.89 and related relations

% pinion, delivery side
Rm1 = sqrt(rho^2 + (rho*nu_m + delta_i1).^2); %4.76 inversa
% pinion, trapped volume side
Rm2_trap = sqrt(rho^2 + (rho*nu_m + delta_i1 + rho*DeltaPhi).^2); %4.84 inversa
% pinion, suction side
Rm2 = sqrt(rho^2 + (TT - delta_i2 - rho*DeltaPhi + rho*nu_a).^2); %4.81 inversa
% internal gear, delivery side
Rc1 = sqrt(rho2^2 + (rho*nu_m + delta_i1 + (rho2 - rho)*tan(thetak)).^2); %4.86 inversa
% internal gear, trapped volume side
Rc2_trap = sqrt(rho2^2 + (rho*nu_m + delta_i1 + (rho2 - rho)*tan(thetak) + rho*DeltaPhi).^2);
%4.87 inversa
% internal gear, suction side
Rc2 = sqrt(rho2^2 + (TT - delta_i2 + rho*nu_a - rho*DeltaPhi + (rho2 - rho)*tan(thetak)).^2);
%4.88 inversa


% 9) VOLUME DERIVATIVES
% Brussani Chapter 4 - case with crescent
dVm_dphi = (b/2) * ( (Rm1.^2 - Re^2) - (Nd/Nd2) * (Rc1.^2 - Rf2^2) );
dVa_dphi = (b/2) * ( (Re^2 - Rm2.^2) - (Nd/Nd2) * (Rf2^2 - Rc2.^2) );
dVt_dphi_raw = (b/2) * ( (Rm2_trap.^2 - Rm1.^2) - (Nd/Nd2) * (Rc2_trap.^2 - Rc1.^2) );

% trapped volume exists only in [phi_bt, phi_et]
mask_trap = is_angle_between(phi, phi_bt, phi_et, DeltaPhi);
dVt_dphi = dVt_dphi_raw;
dVt_dphi(~mask_trap) = 0;

% 10) THEORETICAL FLOW
% Brussani Chapter 4-5:
% Qth(phi) = -omega * [ dVm/dphi + min(dVt/dphi,0) ]
Qth_m3_s = -omega * ( dVm_dphi + min(dVt_dphi, 0) );

% 11) FLOW INDICATORS
Qmean_m3_s = mean(Qth_m3_s);
Qmax_m3_s  = max(Qth_m3_s);
Qmin_m3_s  = min(Qth_m3_s);

Qmean_L_min = Qmean_m3_s * 60 * 1000;
Qmax_L_min  = Qmax_m3_s  * 60 * 1000;
Qmin_L_min  = Qmin_m3_s  * 60 * 1000;

DeltaQ_L_min   = Qmax_L_min - Qmin_L_min;
deltaQ_percent = 100 * DeltaQ_L_min / Qmean_L_min;
```

```
Vg_model_cm3_rev = Qmean_L_min * 1000 / n_rpm;

% 12) COMPARISON WITH MANUFACTURER
err_Vg_percent = 100 * (Vg_model_cm3_rev - Vg_decl_cm3_rev) / Vg_decl_cm3_rev;
err_Q_percent  = 100 * (Qmean_L_min - Q_decl_L_min) / Q_decl_L_min;


% 13) VOLUME RECONSTRUCTION
% purely for visualization
Vm = cumtrapz(phi, dVm_dphi);
Va = cumtrapz(phi, dVa_dphi);

Vt = zeros(size(phi));
if any(mask_trap)
    idx = find(mask_trap);
    Vt(idx) = cumtrapz(phi(idx), dVt_dphi(idx));
    Vt(idx) = Vt(idx) - min(Vt(idx));
end

% 14) RESULTS
fprintf('\n==========================================================\n');
fprintf('THEORETICAL MODEL @ %d rpm\n', n_rpm);
fprintf('==========================================================\n');
fprintf('Mean flow rate              = %.4f L/min\n', Qmean_L_min);
fprintf('Maximum flow rate           = %.4f L/min\n', Qmax_L_min);
fprintf('Minimum flow rate           = %.4f L/min\n', Qmin_L_min);
fprintf('Flow ripple amplitude       = %.4f L/min\n', DeltaQ_L_min);
fprintf('Flow ripple                 = %.3f %%\n', deltaQ_percent);
fprintf('Model displacement          = %.4f cm^3/rev\n', Vg_model_cm3_rev);

fprintf('\n---------------- Manufacturer comparison ----------------\n');
fprintf('Declared displacement       = %.4f cm^3/rev\n', Vg_decl_cm3_rev);
fprintf('Declared flow rate          = %.4f L/min\n', Q_decl_L_min);
fprintf('Displacement error          = %.3f %%\n', err_Vg_percent);
fprintf('Flow rate error             = %.3f %%\n', err_Q_percent);
fprintf('---------------------------------------------------------\n');

fprintf('\n---------------- Crescent angles ----------------\n');
fprintf('chiAS = %.2f deg\n', rad2deg(chiAS));
fprintf('chiAE = %.2f deg\n', rad2deg(chiAE));
fprintf('chiMS = %.2f deg\n', rad2deg(chiMS));
fprintf('chiME = %.2f deg\n', rad2deg(chiME));
fprintf('NOTE: not used in pure theoretical flow.\n');
fprintf('They are used in the full distribution / pressure / leakage model.\n');

% 15) PLOTS
```

```
figure;
plot(rad2deg(phi), Qth_m3_s * 60 * 1000, 'LineWidth', 1.5);
grid on;
xlabel('\phi [deg]');
ylabel('Q_{th} [L/min]');
title(sprintf('Theoretical flow at %d rpm', n_rpm));

figure;
plot(rad2deg(phi), dVm_dphi * 1e9, 'LineWidth', 1.2); hold on;
plot(rad2deg(phi), dVt_dphi * 1e9, 'LineWidth', 1.2);
grid on;
xlabel('\phi [deg]');
ylabel('dV/d\phi [mm^3/rad]');
legend('dV_m/d\phi', 'dV_t/d\phi', 'Location', 'best');
title('Volume derivatives');

figure;
plot(rad2deg(phi), Vm * 1e9, 'LineWidth', 1.2); hold on;
plot(rad2deg(phi), Va * 1e9, 'LineWidth', 1.2);
plot(rad2deg(phi), Vt * 1e9, 'LineWidth', 1.2);
grid on;
xlabel('\phi [deg]');
ylabel('Volume [mm^3]');
legend('V_m', 'V_a', 'V_t', 'Location', 'best');
title('Control volumes');

% 15) ADDITIONAL PLOTS
figure;
plot(rad2deg(phi), rad2deg(nu_m), 'LineWidth', 1.5);
grid on;
xlabel('\phi [deg]');
ylabel('\nu_m [deg]');
title('Auxiliary delivery variable');

figure;
plot(rad2deg(phi), rad2deg(nu_a), 'LineWidth', 1.5);
grid on;
xlabel('\phi [deg]');
ylabel('\nu_a [deg]');
title('Auxiliary suction variable');

figure;
plot(rad2deg(phi), dVa_dphi * 1e9, 'LineWidth', 1.5);
grid on;
xlabel('\phi [deg]');
ylabel('dV_a/d\phi [mm^3/rad]');
title('Derivative of suction volume');
```

```
figure;
plot(rad2deg(phi), dVm_dphi * 1e9, 'LineWidth', 1.5);
grid on;
xlabel('\phi [deg]');
ylabel('dV_m/d\phi [mm^3/rad]');
title('Derivative of delivery volume');

figure;
plot(rad2deg(phi), dVt_dphi * 1e9, 'LineWidth', 1.5);
grid on;
xlabel('\phi [deg]');
ylabel('dV_t/d\phi [mm^3/rad]');
title('Derivative of trapped volume');

% 15) BAR CHART
figure;
bar([Vg_decl_cm3_rev, Vg_model_cm3_rev]);
set(gca, 'XTickLabel', {'Declared V_g', 'Model V_g'});
ylabel('cm^3/rev');
title('Displacement comparison');
grid on;

figure;
bar([Q_decl_L_min, Qmean_L_min]);
set(gca, 'XTickLabel', {'Declared Q', 'Model Q'});
ylabel('L/min');
title(sprintf('Flow rate comparison at %d rpm', n_rpm));
grid on;

% LOCAL FUNCTIONS
function y = evolvente(x)
    y = tan(x) - x;
end

function mask = is_angle_between(phi, a, b, period)
    a = mod(a, period);
    b = mod(b, period);
    phi = mod(phi, period);

    if a <= b
        mask = (phi >= a) & (phi <= b);
    else
        mask = (phi >= a) | (phi <= b);
    end
end
```

Bibliography

[1] M. Rundo and A. Corvaglia, "Lumped Parameters Model of a Crescent Pump," Energies, vol. 9, no. 11, art. 876, 2016.
DOI: 10.3390/en9110876
Link: https://doi.org/10.3390/en9110876

[2] M. Rundo, "Theoretical flow rate in crescent pumps," Simulation Modelling Practice and Theory, vol. 71, pp. 1–14, 2017.
DOI: 10.1016/j.simpat.2016.11.001
Link: https://doi.org/10.1016/j.simpat.2016.11.001

[3] D. Pan and A. Vacca, "Modelling of Crescent-Type Internal Gear Pumps Considering Gear Radial Micromotion," Chemical Engineering & Technology, vol. 46, no. 1, pp. 128–136, 2023.
DOI: 10.1002/ceat.202200419
Link: https://doi.org/10.1002/ceat.202200419

[4] J.-H. Bae and C. Kim, "Design of rotor profile of internal gear pump for improving fuel efficiency," International Journal of Precision Engineering and Manufacturing, vol. 16, pp. 113–120, 2015.
DOI: 10.1007/s12541-015-0014-4
Link: https://doi.org/10.1007/s12541-015-0014-4

[5] S. Guo and X. Guan, "Simulation Research on Trapped Oil Pressure of Involute Internal Gear Pump," Mathematical Problems in Engineering, vol. 2021, Article ID 8834547, 2021.
DOI: 10.1155/2021/8834547
Link: https://doi.org/10.1155/2021/8834547

[6] S. Guo and G. Yu, "Research and design of internal meshing gear pump separating crescent plate," Scientific Reports, vol. 14, art. 3519, 2024.
DOI: 10.1038/s41598-024-53892-6
Link: https://doi.org/10.1038/s41598-024-53892-6

[7] H. Zhou, R. Du, A. Xie, and H. Yang, "Theoretical Analysis for the Flow Ripple of a Tandem Crescent Pump with Index Angles," Applied Sciences, vol. 7, no. 11, art. 1148, 2017.
DOI: 10.3390/app7111148
Link: https://doi.org/10.3390/app7111148

[8] M. Rundo, "Models for Flow Rate Simulation in Gear Pumps: A Review," Energies, vol. 10, no. 9, art. 1261, 2017.
DOI: 10.3390/en10091261
Link: https://doi.org/10.3390/en10091261

[9] M. Brussani, "Profili e Modelli per Pompe ad Ingranaggi Esterni ed Interni"

Acknowledgements

I would like to dedicate this space to everyone who, in various ways, made the completion of this thesis and my Master's degree journey possible.

First and foremost, my sincere gratitude goes to Professor Rundo, for sharing his invaluable knowledge and providing vital guidance throughout the drafting of this work.

A deeply special thank you is dedicated to my family: to my father Mario, my mother Alba, and my brothers Francesco and Valerio. My parents, in particular, have fostered and encouraged my passions and inclinations since childhood. It is solely due to their unwavering support that I am able to achieve this milestone today that is an essential stepping stone toward the fulfilment of my dreams.

An immense gratitude goes to the love of my life, Martina, who remains my daily anchor, supporting me and showing her love every single day. She has always believed in me, even when I struggled to believe in myself. I would like to express my heartfelt appreciation to her entire family for their support, generosity and constant encouragement.

A special mention goes to my little kitten Harry, for his sometimes noisy but indispensable companionship. For keeping me company during late-night studying sessions, and specifically for his contribution of walking across the keyboard to freeze the computer right before I saved, reminding me that sometimes, taking an immediate break is mandatory.

Furthermore, I would like to express my gratitude to all my aunts, uncles, and cousins. While I cannot name each of you individually due to how remarkably large our family is, I am incredibly fortunate for our close-knit bond and grateful for your presence in my life.

I wish to thank my fellow students and companions in this academic adventure, who made the challenges of this journey significantly lighter. Though I have lost touch with some along the way, others continue to be a constant in my life, which brings me immense joy. My thanks also go to my friends outside the university environment and also to my bandmates, Marco and Giuseppe with whom I share one of my greatest passions, music, and with whom I live extraordinary and unforgettable moments.

Last but certainly not least, I extend my heartfelt thanks to all my colleagues, who saw firsthand the hard work, sacrifices, and dedication it took to balance both working and studying over these years.

Finally, I owe a word of thanks to myself: for the perseverance, willpower, and sheer determination that kept me pushing forward. Step by step, but always moving forward.